

1 **Regional Arctic sea-ice prediction: Potential versus**  
2 **operational seasonal forecast skill**

3 **Mitchell Bushuk · Rym Msadek · Michael**  
4 **Winton · Gabriel Vecchi · Xiaosong**  
5 **Yang · Anthony Rosati · Rich Gudgel**

6  
7 Received: date / Accepted: date

8 **Abstract** Seasonal predictions of Arctic sea ice on regional spatial scales are a  
9 pressing need for a broad group of stakeholders, however, most assessments of  
10 predictability and forecast skill to date have focused on pan-Arctic sea-ice ex-  
11 tent (SIE). In this work, we present the first direct comparison of perfect model  
12 (PM) and operational (OP) seasonal prediction skill for regional Arctic SIE within  
13 a common dynamical prediction system. This assessment is based on two com-  
14plementary suites of seasonal prediction ensemble experiments performed with a  
15 global coupled climate model. First, we present a suite of PM predictability ex-  
16periments with start dates spanning the calendar year, which are used to quantify  
17 the potential regional SIE prediction skill of this system. Second, we assess the  
18 system’s OP prediction skill for detrended regional SIE using a suite of retrospec-  
19tive initialized seasonal forecasts spanning 1981-2016. In nearly all Arctic regions  
20 and for all target months, we find a substantial skill gap between PM and OP  
21 predictions of regional SIE. The PM experiments reveal that regional winter SIE  
22 is potentially predictable at lead times beyond 12 months, substantially longer  
23 than the skill of their OP counterparts. Both the OP and PM predictions display  
24 a spring prediction skill barrier for regional summer SIE forecasts, indicating a  
25 fundamental predictability limit for summer regional predictions. We find that a  
26 similar barrier exists for pan-Arctic sea-ice volume predictions, but is not present  
27 for predictions of pan-Arctic SIE. The skill gap identified in this work indicates a  
28 promising potential for future improvements in regional SIE predictions.

---

Mitchell Bushuk  
Geophysical Fluid Dynamics Laboratory, NOAA, Princeton, New Jersey, USA;  
University Corporation for Atmospheric Research, Boulder, Colorado, USA  
E-mail: mitchell.bushuk@noaa.gov

Rym Msadek  
CNRS/CERFACS, CECI UMR 5318, Toulouse, France

Michael Winton, Xiaosong Yang, Anthony Rosati, Rich Gudgel  
Geophysical Fluid Dynamics Laboratory, NOAA, Princeton, New Jersey, USA

Gabriel A. Vecchi  
Department of Geosciences, Princeton University, Princeton, NJ, USA; Princeton Environ-  
mental Institute, Princeton University, Princeton, NJ, USA

29 **Keywords** Sea ice · Seasonal predictability · Arctic

## 30 1 Introduction

31 Rapid changes in Arctic sea-ice extent (SIE), thickness (SIT), and age over the  
32 satellite era, and their implications for a broad group of stakeholders, have led to  
33 a burgeoning research interest in seasonal-to-interannual predictability and pre-  
34 diction skill of Arctic sea ice. Over the past decade, substantial progress in sea-ice  
35 prediction science has been made, including the first seasonal predictions of sea ice  
36 made using coupled global climate models (GCMs) [75, 18, 65, 52, 54, 59, 7, 20, 33, 27,  
37 12, 5, 15], the first prognostic estimates of potential sea-ice prediction skill using  
38 “perfect model” approaches [45, 35, 6, 70, 30, 21, 22], diagnostic studies quantifying  
39 timescales and identifying key sources of sea-ice predictability [44, 4, 36, 17, 21, 11,  
40 9, 16, 13, 10], the development of novel statistical techniques for sea-ice forecasting  
41 [29, 28, 50, 71, 68, 63, 43, 74, 81, 77, 60], and the creation of the sea-ice prediction net-  
42 work (SIPN, [68, 7]), which collects and communicates predictions of September  
43 Arctic SIE (see <http://www.arcus.org/sipn/sea-ice-outlook>).

44 A crucial finding that has emerged from this body of work is that current sea-  
45 sonal forecasts of pan-Arctic SIE made with operational (OP) prediction systems  
46 could be substantially improved. State-of-the-art dynamical prediction systems,  
47 based on fully-coupled GCMs and initial conditions (ICs) constrained by observa-  
48 tions, can skillfully predict detrended pan-Arctic summer SIE at 1-6 month lead  
49 times and winter SIE at 1-11 month lead times depending on the prediction system  
50 used [75, 18, 65, 52, 54, 59, 7, 20, 33, 27]. These OP skill estimates are based on retro-  
51 spective predictions (hindcasts), in which the fixed prediction system is run using  
52 only data available prior to the forecast initialization date. Perfect model (PM)  
53 studies, based on ensembles of model runs initialized from nearly identical ICs,  
54 complement these findings by providing estimates of the upper limits of prediction  
55 skill within a given GCM. These idealized experiments provide skill estimates in  
56 the case of perfectly known model physics and perfect ICs, and therefore are con-  
57 sidered to be an upper bound to the prediction skill achievable in an OP system.  
58 PM studies show that pan-Arctic SIE and sea-ice volume (SIV) are predictable at  
59 12-36 and 24-48 month lead times, respectively, highlighting a significant skill gap  
60 between PM and OP predictions [45, 35, 6, 70, 30, 21].

61 The principal focus of Arctic sea-ice predictability research has been pan-  
62 Arctic SIE, a quantity of minimal utility at stakeholder-relevant spatial scales. As  
63 prospects for skillful seasonal sea-ice prediction systems become more realistic, it is  
64 paramount for sea-ice predictability science to address the regional scales required  
65 by future forecast users, which include northern communities, shipping industries,  
66 fisheries, wildlife management organizations, ecotourism, and natural resource in-  
67 dustries [42]. Initial steps towards understanding Arctic regional predictability  
68 have been made, but many knowledge gaps remain. The PM study of [21] demon-  
69 strated a potential for skillful regional SIE predictions in the HadGEM1.2 GCM,  
70 finding greatest predictability for winter SIE in the Labrador, Greenland-Iceland-  
71 Norwegian (GIN), and Barents Seas (at lead times of 1.5-2.5 years) and lower  
72 predictability for summer SIE (skill at lead times of 2-4 months). [66] showed skill-  
73 ful OP predictions of detrended sea-ice retreat and advance dates, with notably  
74 high skill for ice-advance date predictions in the Labrador Sea/Baffin Bay, Beau-

75 fort Sea, Laptev/East Siberian Seas, Chukchi Sea, and Hudson Bay (3-5 month  
76 leads for detrended anomalies). The work of [46] reported skillful OP predictions  
77 of detrended sea-ice area up to 6 month lead times in the Barents/Kara Seas and  
78 the Northeast passage region. [12] provided the first comprehensive assessment of  
79 OP regional SIE predictions, reporting detrended SIE skill at lead times of 5-11  
80 months in the Labrador, GIN, and Barents Seas, and 1-4 months in the Laptev,  
81 East Siberian, Chukchi, Beaufort, Okhotsk, and Bering Seas. This work attributed  
82 the high winter SIE skill of the North Atlantic to initialization of subsurface ocean  
83 temperature anomalies, and the summer SIE skill to initialization of SIT anom-  
84 lies. Using two different OP seasonal prediction systems, [20] and [27] both found  
85 that improved SIT ICs led to improvements in regional predictions of summer  
86 sea ice. On longer timescales, [80] demonstrated that decadal sea-ice trends in the  
87 North Atlantic are predictable, due to dynamical predictability of thermohaline  
88 circulation variations.

89 While the gap between PM and OP prediction skill suggests a potential for  
90 improved OP predictions, it is important to note that the PM and OP studies  
91 cited above were performed with different GCMs. Since each GCM has unique  
92 model physics and a resulting unique set of model biases, this precludes a direct  
93 quantitative assessment of the PM/OP skill gap. In this study, we present the  
94 first formal comparison of PM and OP Arctic sea-ice prediction skill within the  
95 same GCM-based prediction system. In order to provide an “apples-to-apples”  
96 skill comparison, we first address the general problem of how to make a robust  
97 comparison between PM and OP skill. PM and OP studies often utilize different  
98 metrics to quantify prediction skill, or use different definitions for metrics with  
99 the same name [34]. In this study, we begin by introducing a consistent set of  
100 PM and OP skill metrics, which can be computed analogously for both PM and  
101 OP prediction applications. These metrics are specifically designed to allow for a  
102 robust comparison between PM and OP skill.

103 In this work, we perform a suite of PM experiments initialized from six start  
104 months spanning the calendar year and from six start years spanning different ini-  
105 tial SIV states. This experimental design provides better seasonal coverage than  
106 earlier PM studies, allowing for an evaluation of PM skill for all target months and  
107 lead times of 0-35 months. We also consider a suite of retrospective OP predictions  
108 made with the same model, initialized on the first of each month from January  
109 1981–December 2016. Using these complementary experiments, we directly com-  
110 pare PM and OP prediction skill for regional Arctic SIE, providing a quantitative  
111 assessment of the gap between current and potential Arctic seasonal-to-interannual  
112 prediction skill.

113 The plan of this paper is as follows. In section 2, we describe the experimental  
114 design and introduce prediction skill metrics that allow for a direct comparison  
115 between PM and OP skill. Section 3 presents predictability results for pan-Arctic  
116 SIV and SIE. In section 4, comparisons between PM and OP skill are made for  
117 fourteen Arctic regions. We conclude in section 5.

## 2 Experimental Design and Prediction Skill Metrics

### 2.1 The Dynamical Model

This study is based on experiments performed with the Geophysical Fluid Dynamics Laboratory Forecast-oriented Low Ocean Resolution (GFDL-FLOR) GCM. FLOR is a fully-coupled global atmosphere-ocean-sea ice-land model, which employs a relatively high resolution of  $0.5^\circ$  in the atmosphere and land components and a lower resolution of  $1^\circ$  in the ocean and sea-ice components [72]. The choice of a coarser resolution for the ocean and sea-ice components was made for computational efficiency, as this model was developed for seasonal prediction applications requiring ensemble integrations and many start dates, and for consistency with the ocean and sea ice components of GFDL-CM2.1 [23], which is the basis of the assimilation system with which the initial conditions for the OP predictions are generated. The sea-ice component of FLOR is the sea-ice simulator version 1 (SIS1, [23]), which utilizes an elastic-viscous-plastic rheology to compute the internal ice stresses [37], a modified Semtner 3-layer thermodynamic scheme with two ice layers and one snow layer [78], and a subgrid-scale ice-thickness distribution with 5 thickness categories [2]. FLOR’s ocean component is the Modular Ocean Model version 5 (MOM5, [31]), which uses a rescaled geopotential height coordinate ( $z^*$ , [32]) with 50 vertical levels. The atmospheric component of FLOR is Atmospheric Model version 2.5 (AM2.5, [24]), which uses a cubed-sphere finite-volume dynamical core [49,62] with 32 vertical levels, and the land component of FLOR is Land Model, version 3 (LM3, [53]).

### 2.2 The Control Integration

The perfect model (PM) experiments described in the following subsection are branched from a 300-year control integration of FLOR, which uses radiative forcing and land use conditions that are representative of 1990. This 300-year control integration (“the new control run”) was initialized from year 800 of another 1400-year 1990 control run (henceforth “the original control run”), which had been previously run on a now-decommissioned high-performance computing cluster. The new control run and PM experiments were run on a new computing cluster, which does not bitwise reproduce numerical solutions obtained on the previous cluster but does reproduce the climate mean state and variability. The original control run shows clear signs of model spin up, with a notable adjustment occurring in the first 500 years of the run (see the evolution of SIV anomalies in Fig. 1a). After roughly year 600, the model reaches a statistically steady equilibrium for the variables of interest in this study. The new control run was initialized from the well-equilibrated year 800 of the original control run, and does not show signs of model drift over the 300-year integration period (see Fig. 1a). Centennial-timescale drift of Arctic SIE and SIV associated with model spin up is a ubiquitous feature across GCMs (e.g., see Fig. 1 of [22]) and has the potential to significantly bias PM skill results. These potential skill biases are particularly relevant for regional sea ice, as a drifting climatology can cause a formerly high-variability region to shift to a low-variability region as it becomes ice covered or ice free, and vice versa. Therefore, the well-equilibrated control run shown in Fig. 1a is a crucial feature

of this regional sea-ice study. Henceforth, we will refer to the new 300-year control run simply as “the control run.”

We evaluate the FLOR sea-ice model biases using monthly-averaged passive microwave satellite SIC observations from the National Snow and Ice Data Center (NSIDC) processed using the NASA Team Algorithm (dataset ID: NSIDC-0051, [14]). We also consider SIT data from the Pan-Arctic Ice Ocean Modeling and Assimilation System (PIOMAS, [82]), an ice-ocean reanalysis that agrees quite well with available in situ and satellite thickness observations [64]. For comparison with FLOR, both the NSIDC and PIOMAS data were regridded onto the FLOR sea-ice grid. The pan-Arctic SIE climatology of FLOR has fairly good agreement with satellite observations, with a slight low bias in August–October and good agreement in other months (see Fig. S1a). The model biases are more pronounced when considering SIC spatial patterns. FLOR’s winter SIC has negative biases (too little sea ice) in the Labrador, Okhotsk, and Bering Seas, and positive biases (too much sea ice) in the Greenland-Iceland-Norwegian (GIN) and Barents Seas (Fig. S2a-c). The summer SIC pattern is dominated by a negative bias wrapping the Alaskan and Eurasian coastlines, and a positive bias in the northern GIN and Barents Seas (Fig. S2d-f). Compared to PIOMAS, FLOR has a substantial thin bias of 0.5–1m at most central Arctic gridpoints (Fig. S3) and a lower pan-Arctic SIV in all months of the year (Fig. S1b). The spatial biases in SIC variability are largely dictated by biases in the mean ice-edge position, which result in dipole bias patterns in the SIC standard deviation fields (Fig. S4). One notable exception to this is the Labrador Sea during winter, in which FLOR has less SIC variability throughout the region.

### 2.3 Perfect Model Predictability Experiments

The 300-year control simulation serves as the baseline for our PM predictability experiments. Using this run, we choose a number of start dates, initialize a twelve-member initial condition ensemble for each start date, and run these ensembles forward in time for three years. A novel aspect of our experimental design is the choice of start dates with uniform seasonal coverage. Prior PM studies have focused primarily on January, May, and July start dates [22]. In this study, for each start year, we initialize ensembles on January 1, March 1, May 1, July 1, September 1, and November 1 (see Table 1 for a summary of the PM experiments). This uniform seasonal coverage allows us to investigate the lead-dependence of seasonal forecast skill and to make a clean quantitative comparison with the OP prediction skill reported in [12]. These start dates also allow us to identify optimal initialization months for given regions or target months of interest. In order to assess how predictability varies with the initial SIV state, we choose start years based on SIV anomalies, selecting two high volume years, two typical volume years, and two low volume years. The high/low volume years are years in which the SIV anomaly exceeds  $\pm 1.2\sigma$  in all months of the year, and the typical volume years have SIV anomalies with absolute value less than  $0.25\sigma$  in all months of the year (see Fig. 1b). The SIV standard deviation of the FLOR control run ( $\sigma = 1.1e12 \text{ m}^3$ ) is comparable to the detrended SIV standard deviation of PIOMAS ( $\sigma = 1.3e12 \text{ m}^3$ ), indicating that the chosen high/low SIV anomalies have similar magnitude to those in the PIOMAS record. The start years are chosen at least 20 years apart,

**Table 1** Summary of GFDL-FLOR PM experiments

Start year	Volume State	Start Months	Ensemble members	Integration time
839	High	Jan, Mar, May, Jul, Sep, Nov	12	3 years
874	Low	Jan, Mar, May, Jul, Sep, Nov	12	3 years
898	Typical	Jan, Mar, May, Jul, Sep, Nov	12	3 years
933	High	Jan, Mar, May, Jul, Sep, Nov	12	3 years
981	Low	Jan, Mar, May, Jul, Sep, Nov	12	3 years
1008	Typical	Jan, Mar, May, Jul, Sep, Nov	12	3 years

so that each start year of ensembles can be considered independent of other start years.

A key aspect of PM experiments is the availability of model restart files which can be used to construct an ensemble of initial conditions. In the control run, restart files were saved at monthly frequency, which allows us to initialize an ensemble from any month of the year. The ensembles were constructed by adding a random spatially uncorrelated Gaussian perturbation with standard deviation  $10^{-4}\text{K}$  to the SST field at each ocean gridpoint. This ensemble generation technique mirrors the protocol used in the APPOSITE experiments [21, 70, 22]. Our PM experiments were run with 12 ensemble members, which is the ensemble size used for GFDL’s initialized seasonal predictions (see following subsection). This suite of experiments, consisting of six start years, six start months per start year, 12 ensemble members per start month, and 3 years of integration time, totals 1296 years of model integration.

In each ensemble experiment, the ensemble members are initialized infinitesimally close to one another and diverge over time due to the chaotic dynamics of the system (see Fig. 1c). The rate at which this ensemble divergence occurs provides information on the inherent predictability of the system, quantifying the timescale at which a skillful prediction could be made in the case of perfect ICs and perfectly known model physics. In subsection 2.6, we present a set of metrics used to quantify the prediction skill of PM predictability experiments.

## 2.4 Retrospective Seasonal Prediction Experiments

As a complement to the PM experiments, we analyze the seasonal prediction skill of a suite of retrospective OP prediction experiments made using the FLOR model. These twelve-member ensemble predictions are initialized on the first of each month from January 1981–December 2016, and integrated for one year. The initial conditions come from GFDL’s Ensemble Coupled Data Assimilation (ECDA; [83, 84]) System, which is based on the ensemble adjustment Kalman filter [1]. The ECDA system assimilates satellite sea-surface temperatures (SST), subsurface temperature and salinity data, and atmospheric reanalysis data from National Centers for Environmental Prediction [12]. Note that while this system does not explicitly assimilate sea-ice data, the sea-ice state in the coupled assimilation is constrained via surface heat fluxes associated with assimilation of SST and surface-air temperature data. This assimilation system captures the climatology, long-term trend, and interannual variability of pan-Arctic SIE with reasonable fidelity [54]. These FLOR retrospective seasonal predictions have been used to ex-

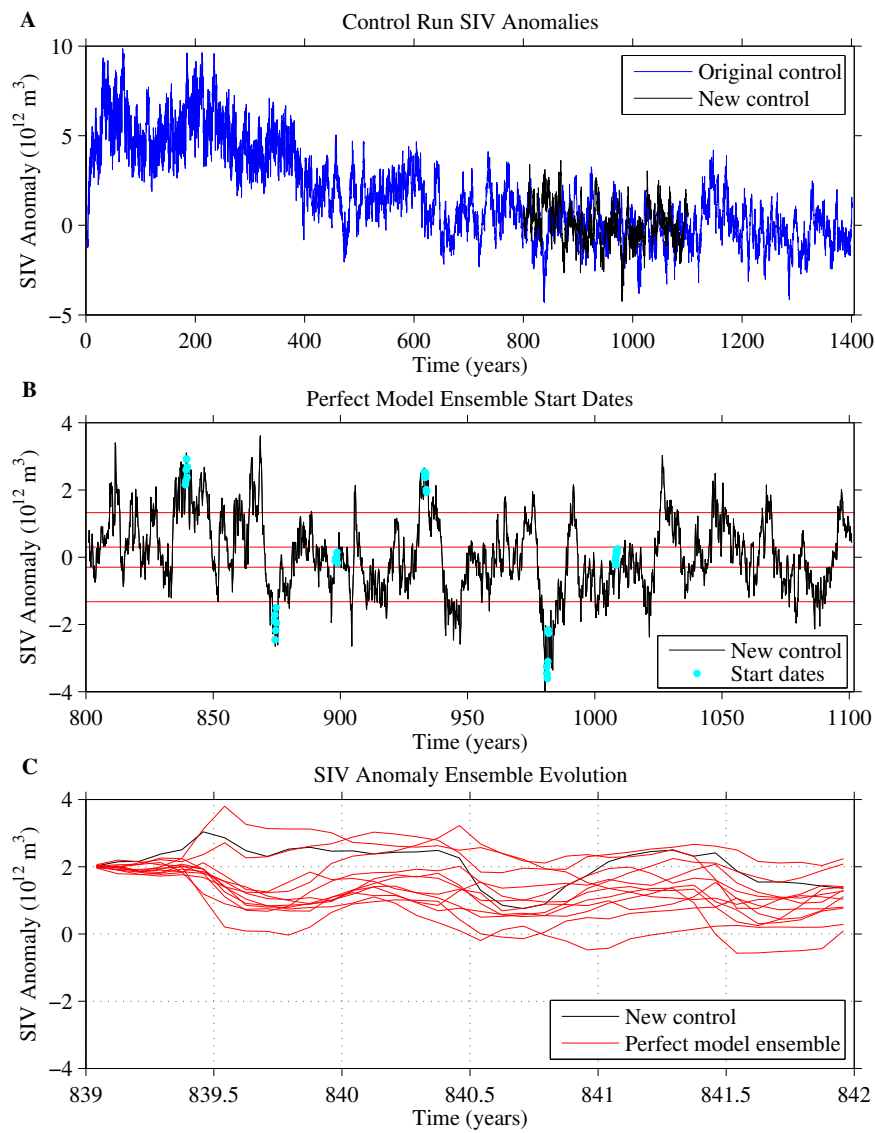


**Fig. 1** Experimental setup for PM experiments. (A): Arctic SIV anomaly timeseries from the original and new 1990 control runs. The new control is initialized from year 800 of the original control. (B): Start dates for PM ensemble experiments (cyan dots). The new control is used to define thresholds to select high/low/typical SIV years. The  $\pm 1.2\sigma$  levels and  $\pm 0.25\sigma$  levels are indicated by horizontal red lines. (C): Evolution of volume anomalies from an ensemble initialized on January 1 of year 839. The black line shows the control run realization.

amine pan-Arctic [54] and regional [12] SIE prediction skill in addition to a diverse set of other climate prediction applications, including regional SST [67], tropical cyclones [72,55], temperature and precipitation over land [39,38], and extratropical storm tracks [79]. Using FLOR for both the PM and OP predictions allows us to make a clean “apples-to-apples” comparison between operational and potential prediction skill within the same prediction system.

## 2.5 Operational Prediction Skill Metrics

We assess the skill of the OP predictions using the anomaly correlation coefficient (ACC) and the mean-squared skill score (MSSS). We let  $o$  and  $p$  be observed and predicted values, respectively, of a time series of interest, for example pan-Arctic SIE. We let  $\tau$  be the forecast lead time,  $o_j$  be the observed value at time  $j$ ,  $K$  be the number of years in the observed timeseries, and  $N$  be the number of prediction ensemble members. We let  $p_{ij}(\tau)$  be the predicted value given by the  $i$ th ensemble member initialized  $\tau$  months prior to time  $j$ . Our lead  $\tau$  prediction of  $o_j$  is given by the ensemble-mean prediction  $\langle p_j(\tau) \rangle$ , where:

$$\langle p_j(\tau) \rangle = \frac{1}{N} \sum_{i=1}^N p_{ij}(\tau). \quad (1)$$

We let  $\bar{\cdot}$  denote the time-mean over the  $K$  samples. The ACC is given by the Pearson correlation coefficient between the predicted and observed timeseries:

$$ACC(\tau) = \frac{\sum_{j=1}^K (\langle p_j(\tau) \rangle - \overline{p(\tau)}) (o_j - \bar{o})}{\sqrt{\sum_{j=1}^K (\langle p_j(\tau) \rangle - \overline{p(\tau)})^2} \sqrt{\sum_{j=1}^K (o_j - \bar{o})^2}}. \quad (2)$$

The mean-squared error (MSE) is given by

$$MSE(\tau) = \frac{\sum_{j=1}^K (\langle p_j(\tau) \rangle - o_j)^2}{K}, \quad (3)$$

and the MSE of a climatological forecast  $\bar{o}$  is given by

$$MSE_{clim} = \frac{\sum_{j=1}^K (\bar{o} - o_j)^2}{K}. \quad (4)$$

The MSSS [56] is a skill score based on a comparison between  $MSE$  and  $MSE_{clim}$ , and is given by

$$MSSS(\tau) = 1 - \frac{MSE(\tau)}{MSE_{clim}}. \quad (5)$$

The MSSS is directly related to the ACC via the decomposition of [56], which shows that

$$MSSS(\tau) = ACC^2(\tau) - \left( ACC(\tau) - \frac{\sigma_p}{\sigma_o} \right)^2 - \frac{(\overline{p(\tau)} - \bar{o})^2}{\sigma_o^2}, \quad (6)$$

where the last two terms are negative definite and correspond to the conditional and unconditional forecast biases, respectively, and  $\sigma$  is the standard deviation of

269 the given time series. The unconditional bias term is related to the mean offset  
 270 between the observed and predicted time series, whereas the conditional bias term  
 271 represents the degree to which the slope of the regression line between these time  
 272 series deviates from 1 (i.e. the degree to which predictions are underconfident or  
 273 overconfident).

274 Since the focus of this study is the initial-value predictability of Arctic sea ice,  
 275 we assess prediction skill relative to a linear trend reference forecast. Specifically,  
 276 we detrend the regional SIE time series' using a linear trend forecast which is  
 277 updated each year using all available past data [60, 12] and compute OP *ACC*  
 278 and MSSS values using these detrended data. This differs from the approach used  
 279 in other hindcast studies, which compute detrended anomalies using linear or  
 280 quadratic trends based on the full hindcast period, providing an *a posteriori* as-  
 281 sessment of detrended prediction skill [75, 18, 65, 52, 54, 59, 33, 27]. A drawback to  
 282 this full-hindcast period approach is that the detrended anomaly of a given year re-  
 283 lies upon future information, and therefore the linear trend reference forecast does  
 284 not represent a viable forecasting strategy. The approach employed here amelio-  
 285 rates this issue, by computing a linear trend forecast each year using all available  
 286 past data (we assume a linear trend of zero for the first three hindcast years).  
 287 After this detrending, the OP *ACC* and MSSS can be cleanly compared to the  
 288 PM *ACC* and MSSS, respectively. Note that we also computed detrended regional  
 289 SIE prediction skill using linear and quadratic trends computed over the full hind-  
 290 cast period, and found that regional prediction skill is relatively insensitive to the  
 291 choice of detrending method.

## 292 2.6 Perfect Model Skill Metrics

293 We next introduce a set of predictability metrics, which are used to judge the  
 294 prediction skill of the PM experiments. These metrics utilize a technique com-  
 295 monly used in the PM literature [19, 34] in which each ensemble member in turn  
 296 is taken to be the “truth” and the remainder of the ensemble is used to predict  
 297 this “truth” member. In order to facilitate a clean comparison between OP and  
 298 PM skill, we define our PM skill metrics in analogy to the OP skill metrics pre-  
 299 sented in the previous section. Note that these metrics differ somewhat from other  
 300 metrics commonly used in the PM predictability literature [19, 61, 34], and offer  
 301 conceptual advantages when comparing to OP prediction skill (see Appendix 6.2  
 302 for a discussion of how these metrics relate to other commonly used definitions). In  
 303 particular, these PM metrics can be compared directly with their OP analogues,  
 304 while other commonly used PM metrics cannot.

305 We let  $x$  be a timeseries of interest, for example pan-Arctic SIE or SIV. We let  
 306  $x_{ij}(\tau)$  be the prediction of  $x$  from start date  $j$  and ensemble member  $i$  at lead time  
 307  $\tau$ . Suppose that we have  $M$  ensemble start dates, with each ensemble consisting  
 308 of  $N$  members (in this study  $M = 6$  and  $N = 12$ ). We now motivate a definition  
 309 for the PM MSE. Suppose that ensemble member  $i$  is the synthetic observation  
 310 (the “truth” member). We use the remaining  $N - 1$  ensemble members to predict  
 311 this synthetic observation. Specifically, we take the ensemble mean of these  $N - 1$   
 312 members as our prediction of  $x_{ij}$ . As a notation, we let  $\mathbf{x}_{\hat{i}j}$  be a vector of ensemble  
 313 members from the  $j$ th ensemble with the  $i$ th member removed:

$$\mathbf{x}_{\hat{i}j} = (x_{1j}, \dots, x_{i-1j}, x_{i+1j}, \dots, x_{Nj}), \quad (7)$$

314 and let  $\langle \cdot \rangle$  denote the ensemble mean operator. Thus,  $\langle \mathbf{x}_{ij}(\tau) \rangle$  is our prediction  
 315 of  $x_{ij}$ , and has a squared error of  $(\langle \mathbf{x}_{ij}(\tau) \rangle - x_{ij}(\tau))^2$ . Letting each ensemble  
 316 member take a turn as the truth and averaging over all ensemble members ( $N$ )  
 317 and ensemble start dates ( $M$ ), we obtain the mean-squared error (MSE):

$$MSE(\tau) = \frac{\sum_{j=1}^M \sum_{i=1}^N \left( \langle \mathbf{x}_{ij}(\tau) \rangle - x_{ij}(\tau) \right)^2}{MN}. \quad (8)$$

318 This metric is the PM analogue to the OP MSE defined in Eqn. 3. This MSE  
 319 formula satisfies a necessary condition for forecast reliability [41, 58, 40, 48, 76],  
 320 which states that the MSE of ensemble-mean forecasts is equal to the mean intra-  
 321 ensemble variance,  $\sigma_e^2$ , up to a scaling factor related to the finite ensemble size.  
 322 Specifically, we show in Appendix 6.1 that

$$MSE(\tau) = \frac{N}{N-1} \sigma_e^2(\tau), \quad (9)$$

323 where

$$\sigma_e^2(\tau) = \frac{1}{M} \sum_{j=1}^M \frac{1}{N-1} \sum_{i=1}^N \left( \langle \mathbf{x}_j(\tau) \rangle - x_{ij}(\tau) \right)^2, \quad (10)$$

324 and  $\langle \mathbf{x}_j(\tau) \rangle$  is the ensemble mean of the  $j$ th ensemble.

325 We can now define a PM MSSS, given by

$$MSSS(\tau) = 1 - \frac{MSE(\tau)}{\sigma_c^2}, \quad (11)$$

326 where  $\sigma_c^2$  is the climatological variance of  $x$  computed from the control run.  $\sigma_c^2$  is  
 327 the  $MSE$  of a climatological reference forecast, which can be seen by replacing the  
 328 ensemble-mean forecast in Eqn. 8 with  $\mu$ , the monthly climatological mean of the  
 329 control run. In practice, computing the climatological variance from the control  
 330 run is more robust than using Eqn. 8, due to the relatively small number of start  
 331 dates used in most PM studies. MSSS values close to one indicate high PM skill  
 332 and a value of zero indicates no prediction skill relative to a climatological forecast.  
 333 The MSSS is closely related to the potential prognostic predictability (PPP, [61]),  
 334 and can be interpreted analogously (see Appendix 6.2).

335 We also consider root-mean squared error (RMSE)

$$RMSE(\tau) = \sqrt{MSE(\tau)}, \quad (12)$$

336 which quantifies the error in physical units, and the normalized RMSE (NRMSE),

$$NRMSE(\tau) = \frac{RMSE(\tau)}{\sigma_c}, \quad (13)$$

337 which normalizes the RMSE by the RMSE of a climatological forecast. NRMSE  
 338 values close to zero indicate skillful PM predictions and a value of one indicates no  
 339 prediction skill relative to a climatological forecast. The MSSS is directly related  
 340 to the NRMSE via

$$MSSS(\tau) = 1 - (NRMSE(\tau))^2. \quad (14)$$

341 This RMSE definition provides a more natural comparison with OP RMSE than  
 342 the definition of [19] (which includes an additional factor of  $\sqrt{2}$ ), reducing potential  
 343 for confusion when interpreting PM RMSE values (see Appendix 6.2).

344 We define the *ACC* as the correlation between predicted and “observed”  
 345 anomalies, where each ensemble member  $x_{ij}$  takes a turn as the “truth” and the  
 346 ensemble means  $\langle \mathbf{x}_{ij}(\tau) \rangle$  are used to predict these synthetic observations:

$$ACC(\tau) = \frac{\sum_{j=1}^M \sum_{i=1}^N \left( \langle \mathbf{x}_{ij}(\tau) \rangle - \mu(\tau) \right) \left( x_{ij}(\tau) - \mu(\tau) \right)}{\sqrt{\sum_{j=1}^M \sum_{i=1}^N \left( \langle \mathbf{x}_{ij}(\tau) \rangle - \mu(\tau) \right)^2} \sqrt{\sum_{j=1}^M \sum_{i=1}^N \left( x_{ij}(\tau) - \mu(\tau) \right)^2}}. \quad (15)$$

347 Note that the anomalies are computed relative to  $\mu(\tau)$ , which is the climatological  
 348 value of  $x$  at lead time  $\tau$  computed using the control run. In a non-stationary  
 349 climate,  $\mu$  is a function of start date  $j$ . Given that the control run considered in  
 350 this study has a statistically steady climate, we drop the  $j$  dependence in this  
 351 formula. *ACC* values near 1 indicate high PM skill, and values of zero indicate no  
 352 skill relative to a climatological forecast.

## 353 2.7 Significance Testing

354 Throughout the manuscript, we assess statistical significance using a 95% confi-  
 355 dence level. The statistical significance of the PM RMSE, NRMSE, and MSSS  
 356 values is assessed using an  $F$ -test based on the  $F_{MN-1, s^*-1}$  distribution, where  
 357  $M$  and  $N$  are the number of start dates and ensemble members from the PM  
 358 experiments, respectively, and  $s^*$  is the effective number of degrees of freedom in  
 359 the control run, given by  $s^* = s \frac{1-r(\Delta t)^2}{1+r(\Delta t)^2}$  where  $s$  is the number of samples in  
 360 the control run and  $r(\Delta t)$  is the lag-1 year autocorrelation computed from the  
 361 control run [8]. For the initialized forecast RMSE, NRMSE, and MSSS values,  
 362 we use an  $F$ -test based on the  $F_{K^*-1, K^*-1}$  distribution. Here  $K^*$  is given by  
 363  $K^* = K \frac{1-r_1(\Delta t)r_2(\Delta t)}{1+r_1(\Delta t)r_2(\Delta t)}$ , where  $K = 35$  is the number of years in the retrospective  
 364 forecast experiments and  $r_1(\Delta t)$  and  $r_2(\Delta t)$  are the lag-1 year autocorrelation  
 365 values for each time series.

366 We assess whether the PM *ACC* values are significantly greater than zero based  
 367 on a  $t$ -test with  $MN - 2$  degrees of freedom. Similarly, we assess the OP *ACC*  
 368 values using a  $t$ -test with  $K^* - 2$  degrees of freedom. Scatterplots of predicted vs  
 369 observed regional SIE show that the assumptions of linearity and homoscedasticity  
 370 are satisfied in all regions except for the Central Arctic, which is fully ice-covered  
 371 for many of the verification years. When directly comparing PM and OP forecast  
 372 ACC, we use the OP forecast significance threshold, which is the higher (more  
 373 conservative) threshold of the two.

### 374 **3 Pan-Arctic Predictability**

#### 375 3.1 Pan-Arctic SIV

376 We begin by investigating the ensemble evolution and PM prediction skill for pan-  
 377 Arctic SIV. As an example, Fig. 2 shows the ensemble evolution of SIV anomalies  
 378 for ensembles initialized in year 839, a high volume year. As the ensembles evolve  
 379 in time, they progressively diverge under the chaotic dynamics of the system. This  
 380 divergence occurs on a timescale of years for pan-Arctic SIV: After three years of  
 381 integration, most ensemble members have retained a portion of their initial posi-  
 382 tive SIV anomaly, indicating that SIV is predictable beyond three-year lead times  
 383 in this model. The rate of ensemble divergence also has a clear seasonal depen-  
 384 dence. In particular, the ensemble members diverge rapidly over the months of  
 385 May–July, and experience a much slower rate of divergence over the late summer,  
 386 fall, and winter months (for example, compare the May initialized ensemble to the  
 387 July initialized ensemble). This qualitative behavior is consistent with the physi-  
 388 cal expectation that the positive ice-albedo feedback should drive rapid ensemble  
 389 divergence during the months of maximum solar insolation. Conversely, negative  
 390 feedbacks active in fall and winter should act to reduce ensemble divergence, pos-  
 391 sibly even leading to ensemble convergence. These feedbacks include the negative  
 392 feedback between ice growth and ocean entrainment ([51], ice growth increases  
 393 the amount of heat entrained into the mixed layer, reducing ice growth rates), ice  
 394 growth and ice thickness ([3], thin ice has larger growth rates than thick ice), and  
 395 ice strength and ice thickness ([57], thin, weak ice has a greater propensity for  
 396 thickening via ice convergence and for open-water formation via ice divergence,  
 397 which leads to increased thermodynamic growth).

398 The PM skill metrics help to quantify the qualitative impressions obtained  
 399 from Fig. 2. In Fig. 3, we plot the PM RMSE, NRMSE, ACC, and MSSS for pan-  
 400 Arctic SIV. Note that each of these curves is computed over all six start years.  
 401 Each of these metrics shows statistically significant prediction skill for SIV to lead  
 402 times beyond 36 months, consistent with earlier PM studies [6, 70, 21, 30, 22]. We  
 403 find that error growth rates and normalized error growth rates, as indicated by the  
 404 slopes of the RMSE and NRMSE curves, respectively, vary strongly with target  
 405 month. For both RMSE and NRMSE, the largest error growth occurs in May–July,  
 406 which is followed by a sharp decrease in error growth in August and September.  
 407 These low error growth rates continue into the fall and winter seasons, reaching  
 408 their lowest values in the months of January–April (the error growth rates are  
 409 negative in the winters of the second and third years). This is followed by rapid  
 410 error growth in May as the melt season begins, and the error growth cycle roughly  
 411 repeats again. Similar behavior is also observed in the *ACC* and *MSSS* metrics,  
 412 with precipitous decreases in skill from May–July and much slower skill declines  
 413 for the remainder of the year. The *MSSS*, and to a lesser extent the *ACC*, display  
 414 a winter reemergence of prediction skill in years two and three, in which the winter  
 415 skill values are higher than the skill of the previous summer.

416 The clear seasonality of SIV error growth rates highlights the crucial impor-  
 417 tance of initialization month in Arctic SIV predictions. In particular, there is a  
 418 significant skill gap between predictions initialized prior to June and those initial-  
 419 ized post June, suggesting a melt season “predictability barrier” for SIV. These  
 420 results demonstrate that this barrier lies somewhere between May 1 and July 1,

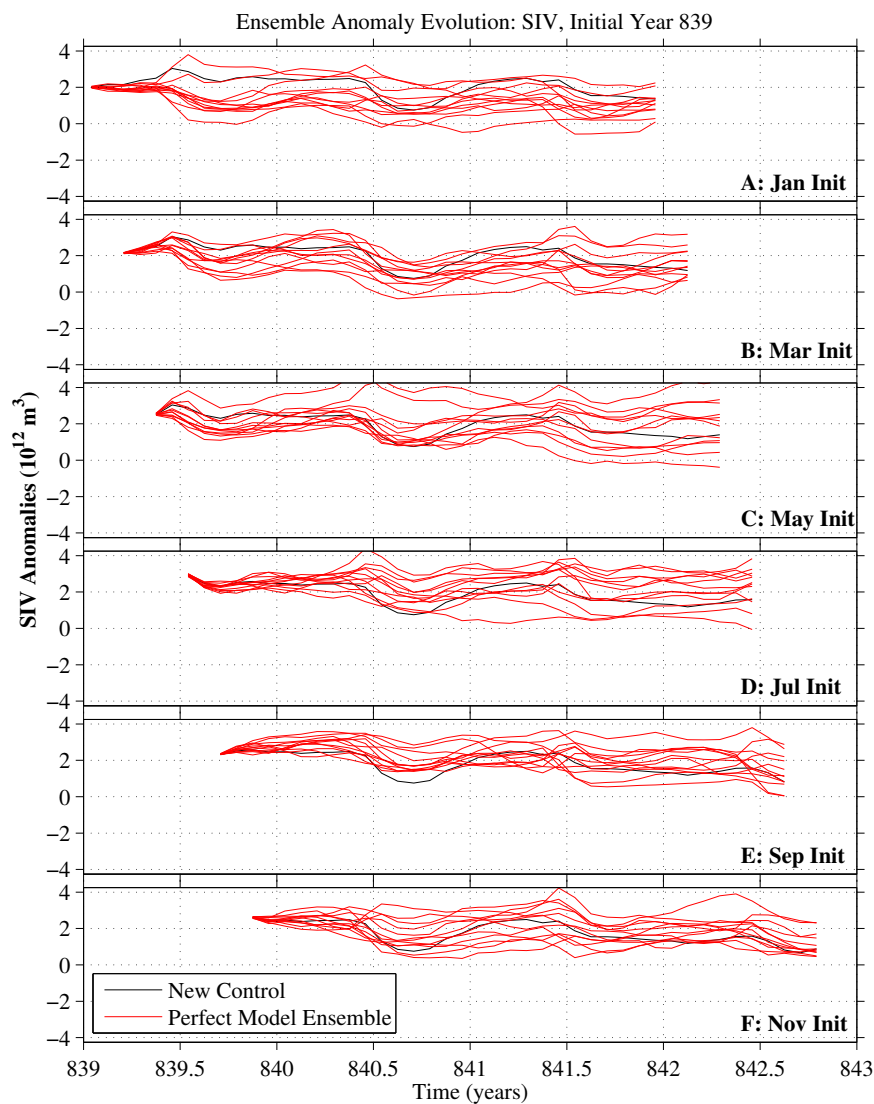


**Fig. 2** Temporal evolution of sea ice volume anomalies for ensembles initialized in year 839 and months (A) January; (B) March; (C) May; (D) July; (E) September; (F) November. The control run realization is shown in black.

421 but further experiments are required to pinpoint its precise date. In other words,  
 422 how far into the melt season must a prediction be initialized in order to avoid the  
 423 unpredictable effects of atmospheric chaos, melt onset variability, and ice-albedo  
 424 feedbacks? It is important to note that while this melt season predictability barrier  
 425 is quite stark for SIV, it is less clearly defined for predictions of pan-Arctic SIE  
 426 (see subsection 3.4, ahead).

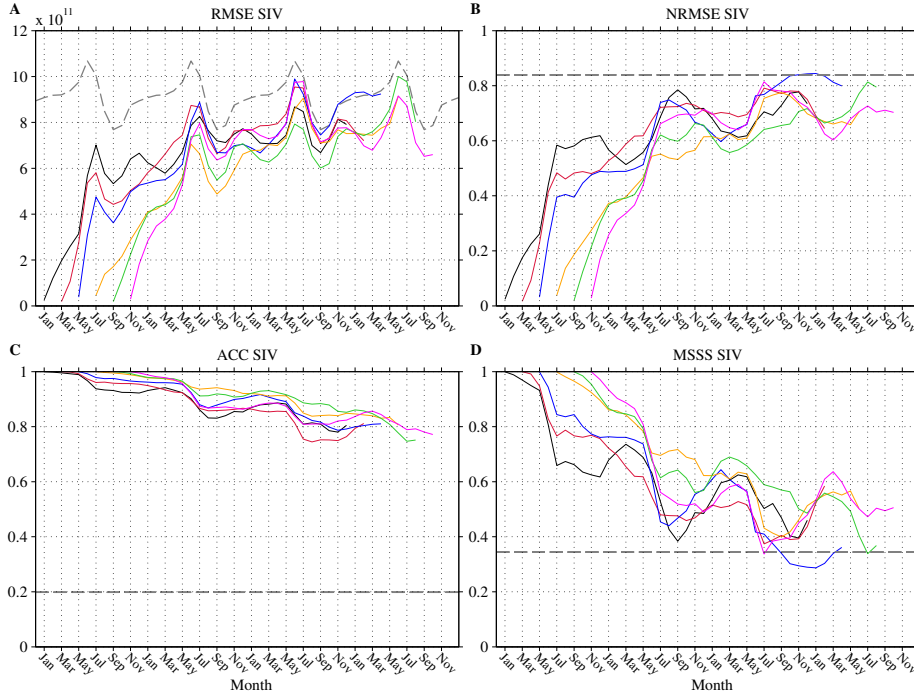


**Fig. 3** Pan-Arctic SIV PM prediction skill for different initialization months. Shown here are the temporal evolutions of (A) RMSE; (B) NRMSE; (C) ACC; and (D) MSSS. The curves are colored based on their initialization month. The gray dashed lines indicate the 95% threshold for statistical significance. Note that the RMSE significance level is not constant due to the seasonal cycle in pan-Arctic SIV standard deviation.

### 427 3.2 State-dependence of predictability

428 Next, we consider the state-dependence of SIV predictability, asking: Does the  
 429 initial SIV state have an influence on SIV predictability characteristics? In Fig. 4,  
 430 we plot SIV predictability metrics for each initial month binned into high, low,  
 431 and typical volume states. For the skill metrics based on ensemble spread (RMSE,  
 432 NRMSE, and MSSS), we find no clear dependence on the volume state; however,  
 433 the *ACC* metric shows a striking difference between the high/low volume states  
 434 and the typical volume states. This result is consistent with the findings of [22]  
 435 and can be explained via the *ACC* formula given in Eqn. 15. For the high/low  
 436 volume ensembles, the ensemble means retain positive/negative anomalies over  
 437 some timescale as the model relaxes towards its climatology (e.g. Fig. 2a), and the  
 438 ensemble members fluctuate randomly around this ensemble mean. Therefore, the  
 439 high/low ensembles each contribute positive values to the numerator of Eqn. 15,  
 440 since both the synthetic observations and synthetic predictions have like-signed  
 441 anomalies. On the other hand, the typical-anomaly ensembles fluctuate randomly  
 442 around a near-zero anomaly state, making both positive and negative contributions  
 443 to the numerator of Eqn. 15, and producing an *ACC* that is close to zero. A similar

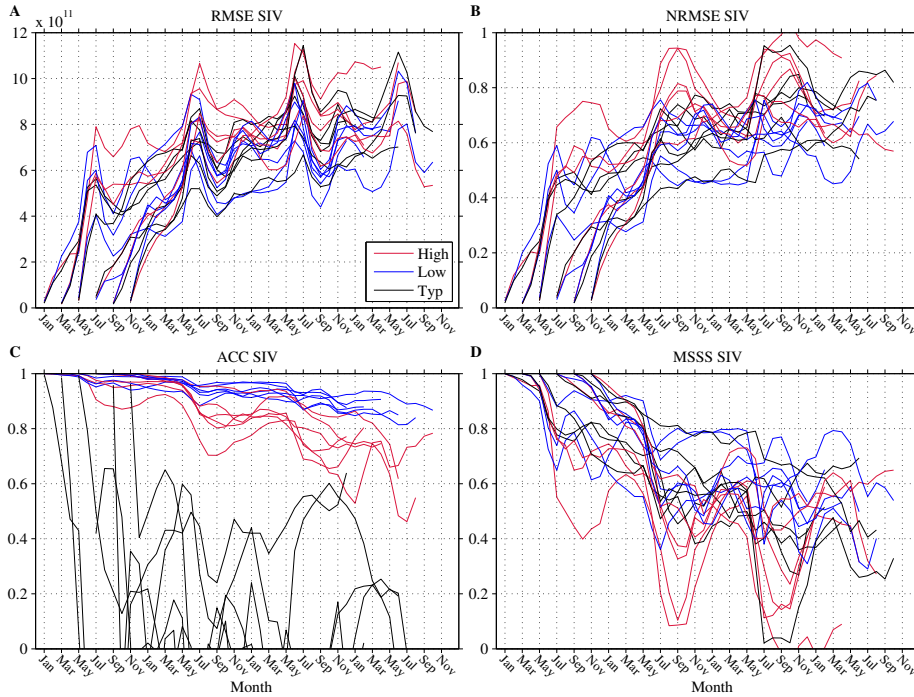


**Fig. 4** PM prediction skill (A: RMSE; B: NRMSE; C: *ACC*; D: MSSS) for pan-Arctic SIV in high (red curves), low (blue curves), and typical (black curves) volume states for different initialization months.

444 *ACC* state-dependency holds for pan-Arctic SIE and other variables (not shown).  
 445

### 446 3.3 An unbiased estimate of perfect model *ACC*

447 Because the PM *ACC* is strongly state dependent, the *ACC* computed using  
 448 Eqn. 15 will be highly sensitive to the set of start dates chosen for a given PM  
 449 study. This is an important caveat to consider when evaluating PM *ACC*: If start  
 450 dates are not drawn randomly from the climatological distribution of states, the  
 451 *ACC* estimates will have systematic biases. For example, in this study, start dates  
 452 were selected specifically to have high, low, and typical volume states (see Fig. 1b).  
 453 These states do not obey the climatological distribution of volume states, as four  
 454 of the six have notably large anomalies. Since large-anomaly states have higher  
 455 *ACC* values, our *ACC* estimates are likely biased high due to the non-random  
 456 sampling of start dates used in this study.

457 To remedy this issue, we appeal to the decomposition of [56], which relates  
 458 the MSSS to the *ACC* (see Eqn. 6). In a PM framework, predictions are free  
 459 of conditional and unconditional biases, therefore [56] suggests that the identity  
 460  $MSSS = ACC^2$  should hold for PM predictions [70,34]. However, we find that  
 461 PM MSSS is not equal to  $ACC^2$  (e.g. see Fig. 6, ahead). Why is this? The

decomposition of [56] is a mathematical identity, which holds identically when the climatological mean and variance are computed “in sample” (i.e. using the available samples from the PM experiments, and not the control run values). In Eqns. 11 and 15, the climatological mean and variance are computed using the control run. If the start dates are non-randomly sampled, the control run mean and variance will be biased relative to the “in sample” mean and variance. This results in a breakdown of the decomposition of [56]. Since the *MSSS* shows much less sensitivity to start date than the *ACC*, it is less prone to sampling bias, and provides a more robust assessment of PM skill. We use this fact to define an unbiased estimate of the *ACC*,  $ACC_U$ , which can be cleanly compared to OP *ACC* values:

$$ACC_U = \sqrt{MSSS}. \quad (16)$$

The  $ACC_U$  is the value the *ACC* would have if the decomposition of [56] held, which is the case when the PM states are sampled from the climatological distribution. Therefore, up to the independence of *MSSS* with respect to start date, this formula provides an *ACC* estimate which is insensitive to start-date sampling error. In the following section, we directly compare OP *ACC* and PM  $ACC_U$ . Note that we could also directly compare OP and PM predictions based on *MSSS* values. If this comparison is made, many of the skill structures present in OP *ACC* are degraded and the PM/OP skill gap is larger than the gap based on *ACC*, due to conditional biases in the OP predictions (not shown). For these reasons, we make our skill comparisons using OP *ACC*, which provides a lower bound on the PM/OP skill gap.

### 3.4 Pan-Arctic SIE predictability

In this subsection, we compare the PM and OP prediction skill of pan-Arctic SIE. Figure 5 shows the evolution of RMSE, NRMSE, *ACC*, and *MSSS* for different initialization months for both PM and OP predictions of pan-Arctic SIE. Figure 6 takes a different vantage point, plotting the skill as a function of target month (the month we are trying to predict) and forecast lead time. These “target month” style PM skill plots are a unique contribution of this study, made possible by our choice of equally-spaced initialization months spanning the calendar year. Previous PM studies have typically focussed on January and/or July initializations, not providing enough initial-month “resolution” to construct a target-month style plot. These plots allow for a systematic study of the skill dependence on target month, initial month, and lead time. Note that we have PM predictions initialized at two-month intervals. For example, for target month January, we have predictions for all even lead times, from lead-0 through lead-34 (note that a lead-0 prediction is defined as the January-mean value from a prediction initialized on January 1). To obtain skill estimates for the odd lead times, we perform a linear interpolation between the even-lead values. This method provides reasonable results, as most skill variations occur over lead times of many months (see Fig. 6).

We find a striking gap between the PM and OP prediction skill for pan-Arctic SIE. While the OP predictions have statistically significant *ACC* at lead times of 0–5 months depending on the target month (Fig. 6c), the PM predictions have statistically significant *ACC* and  $ACC_U$  up to lead times of 35 months, for all

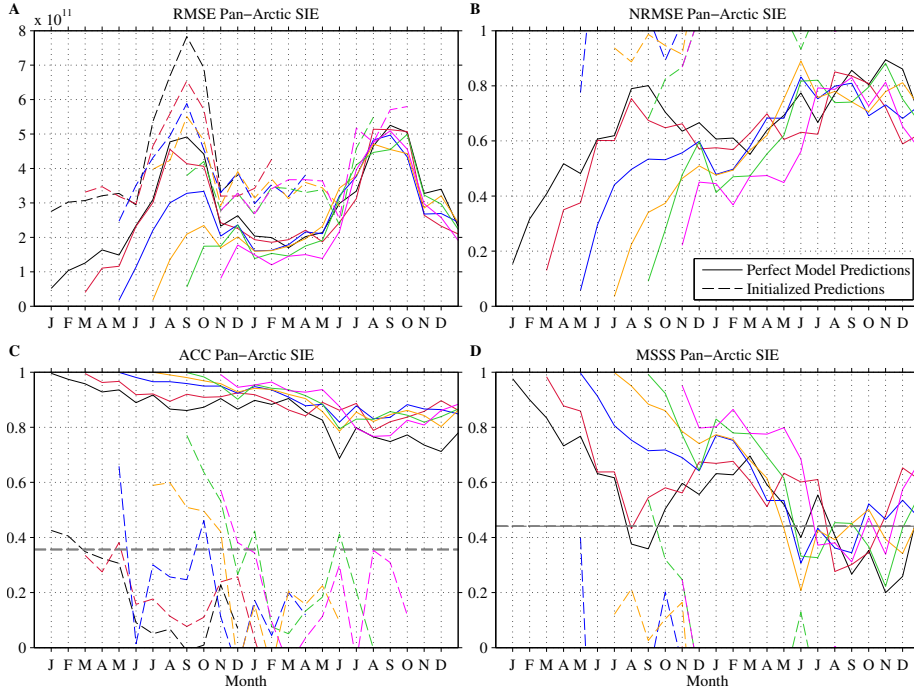


**Fig. 5** Comparison of PM (solid lines) and OP (dashed lines) prediction skill (A: RMSE; B: NRMSE; C:  $ACC$ ; D: MSSS) for pan-Arctic SIE for different initialization months. The 95% significance levels for  $ACC$  and MSSS are plotted as dashed gray lines.

506 target months (Fig. 6a,b). It is important to note that PM skill should be consid-  
 507 ered an upper limit of prediction skill, and may overestimate the skill achievable  
 508 in reality (see discussion in Section 4.3, ahead). Nevertheless, the skill gap shown  
 509 in Fig. 5 and 6 suggests that substantial skill improvements are possible in current  
 510 OP prediction systems. In particular, Fig. 5 shows large differences in lead-0 skill,  
 511 indicating that the OP predictions likely suffer from initialization errors and/or  
 512 initialization shocks. These lead-0 predictions could presumably be improved by  
 513 assimilating more observational data, improving data assimilation techniques, and  
 514 expanding existing observational networks. In addition, we find that the loss of  
 515 skill in the OP predictions occurs much more rapidly than in the PM experiments.  
 516 This rapid loss of skill likely results from a combination of i) model physics errors;  
 517 ii) model drift associated with initialization shock; and iii) differences between  
 518 the model and nature in their underlying predictability, possibly resulting in an  
 519 overestimated upper limit of predictability in the PM experiments.

520 Comparing Fig. 6a and 6b, we find that pan-Arctic SIE  $ACC$  is higher than  
 521  $ACC_U$ , consistent with our *a priori* expectation from subsection 3.3.  $ACC$  and  
 522  $ACC_U$  offer similar qualitative conclusions, but have quantitative differences when  
 523 assessing limits of predictability. For the skill comparisons throughout the remain-  
 524 der of the paper, we will use the  $ACC_U$  values when comparing to OP prediction  
 525  $ACC$ . The PM skill shows a clear seasonality, with higher skill for winter SIE pre-  
 526 dictions than summer SIE. As a reference-level for a “highly skillful” prediction,

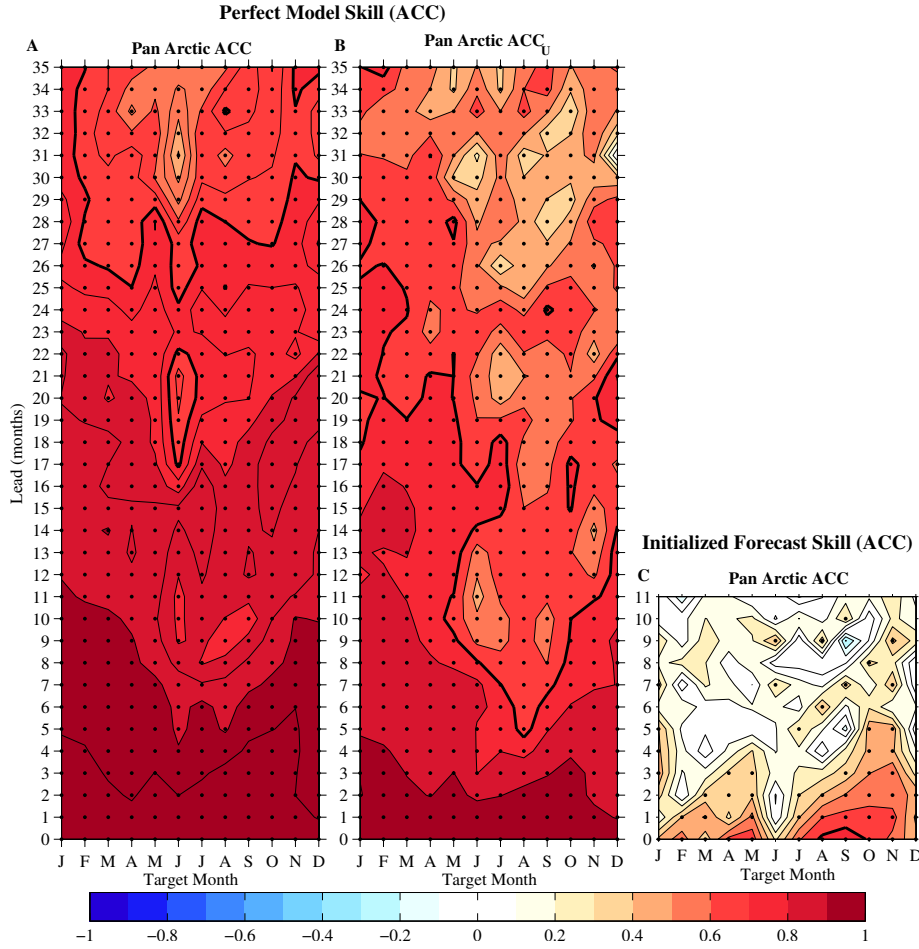


**Fig. 6** Comparison of PM and OP prediction skill for pan-Arctic SIE, plotted as a function of target month and forecast lead time. Panel A shows PM  $ACC$  computed using Eqn. 15, Panel B shows PM unbiased  $ACC$ , defined as  $ACC_U = \sqrt{MSSS}$ , and Panel C shows  $ACC$  from the OP prediction experiments. The thick black lines indicate the  $ACC=0.7$  contours. Dots indicate months in which the  $ACC$  values are statistically significant at the 95% confidence level.

527 we have marked the  $ACC = 0.7$  contour in Fig. 6, as this is the level at which half  
 528 the variance of the observed signal can be predicted. This shows that half the winter  
 529 SIE variance is predictable at 18-26 month lead times, whereas the analogous  
 530 limits for summer SIE are 5-11 months.

531 The study of [21] found evidence of a May “predictability barrier” for pan-  
 532 Arctic SIE, in which predictions initialized in May lost skill more rapidly in the  
 533 first four months than those initialized in January or July. In this model, there is no  
 534 clear evidence of such a barrier, as the error growth rates over the first four months  
 535 are similar for all initialization months (see Fig. 5b,d). Also, a May predictability  
 536 barrier would result in a diagonal  $ACC_U$  feature corresponding to initial month  
 537 May in Fig. 6b, which is not seen. This lies in contrast to SIV, which shows clear

538 evidence of a melt-season predictability barrier (see Fig. 3). Interestingly, the OP  
 539 predictions of summer SIE show evidence of a spring prediction skill barrier, with  
 540 lower skill for forecasts initialized prior to May. A similar feature is also seen in  
 541 SIE persistence forecasts (see Fig. S8), suggesting that SIE persistence is a key  
 542 source of skill for the OP predictions, whereas the PM predictions presumably  
 543 benefit from other sources of predictability, such as perfect SIT ICs, which extend  
 544 skill beyond this barrier. We find that both PM and OP predictions show spring  
 545 skill barriers in certain regions, which we explore in Section 4 ahead.

## 546 4 Regional Sea-Ice Predictability

### 547 4.1 SIC Predictability

548 In this section, we move to smaller spatial scales, exploring the ability of this  
 549 model to make skillful predictions at the regional and gridpoint scale. In Fig. 7,  
 550 we plot PM MSSS values for SIC for different target months and lead times of 0–14  
 551 months. We find that for all target months, the lead-0 SIC predictions are highly  
 552 skillful, indicating a year-round potential for regional-scale sub-seasonal sea-ice  
 553 predictions in this model. The loss of SIC predictability with lead time is highly  
 554 dependent on the region and target month. We observe a clear difference between  
 555 summer and winter SIC predictions, with summer predictions losing most of their  
 556 skill beyond six-month lead times and winter predictions retaining skill beyond  
 557 14-month lead times. This long-lead winter prediction skill is notably high in the  
 558 Barents and GIN Seas, with lower values in the Labrador, Bering, and Okhotsk  
 559 Seas. The SIC prediction skill for even target months and odd lead times has  
 560 analogous skill characteristics (not shown).

561 To synthesize the information of Fig. 7, we introduce a “predictable area”  
 562 metric, defined as

$$\text{Predictable area}(\tau) = \frac{\int MSSS(x, y, \tau) dA}{\int MSSS(x, y, \tau = 0) dA}, \quad (17)$$

563 which is the area integral of the SIC MSSS for a given target month, normalized by  
 564 its lead-0 value. Fig. 8 shows the evolution of SIC predictable area with lead time.  
 565 We find that predictions of summer and winter SIC lose predictability at a similar  
 566 rate over the first 3 months, after which the rates of predictability loss begin to  
 567 diverge. At lead times beyond 6 months, the winter SIC predictions (target months  
 568 December–May) have higher predictable area values than summer SIC predictions  
 569 (target months June–November). Consistent with the pan-Arctic SIE results, this  
 570 shows that there is a greater potential for skillful long-lead predictions of winter  
 571 SIC compared with summer SIC.

### 572 4.2 Regional SIE predictability

573 Next, we consider the predictability of regional SIE, providing a direct comparison  
 574 between PM and OP regional SIE prediction skill. Regional SIE is likely a more  
 575 “forgiving” metric than SIC, as it is less sensitive to local-scale ice dynamics asso-  
 576 ciated with unpredictable atmospheric forcing. The region definitions follow those

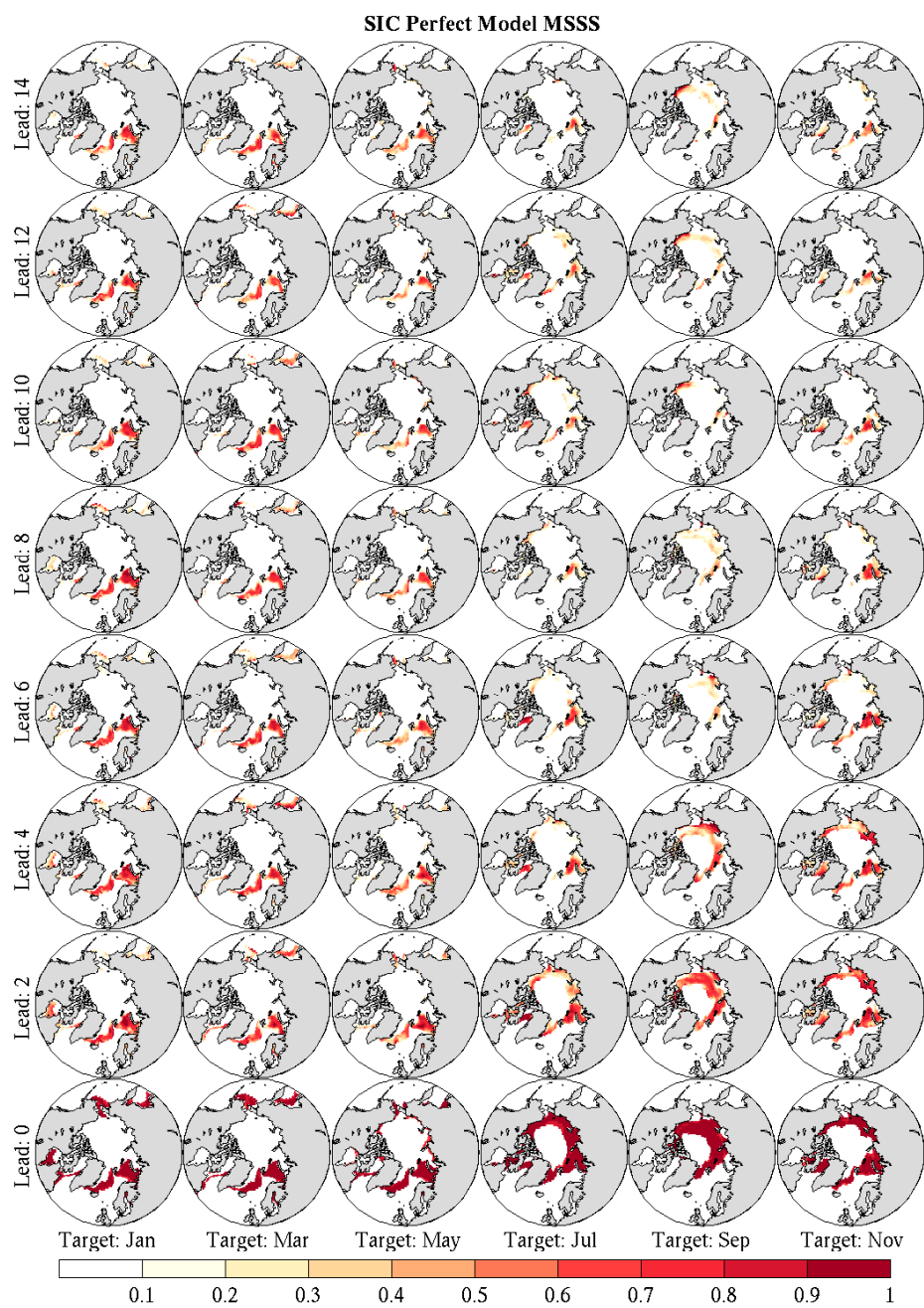


**Fig. 7** SIC PM MSSS for different target months and lead times of 0–14 months. A mask has been applied such that only gridpoints with SIC standard deviation greater than 10% are plotted.

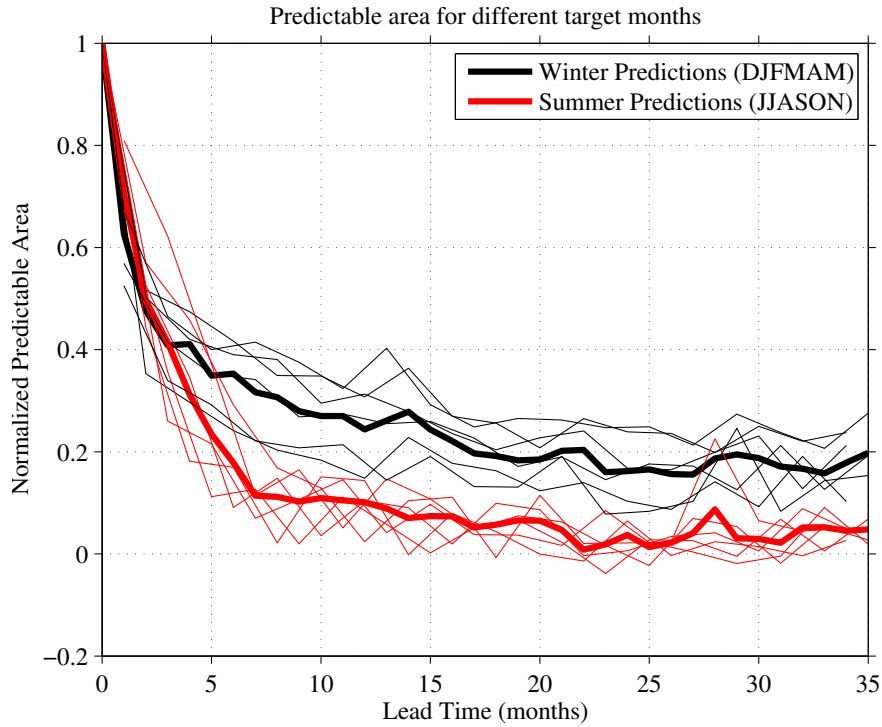


**Fig. 8** SIC predictable area (see Eqn. 17) vs lead time. Each winter target month (December–May) is plotted as a thin black curve and each summer target month (June–November) is plotted as a thin red curve. The thick black and red curves are the mean over all winter and summer target months, respectively.

577 used in [21,12] (See Fig. S5). We find that for nearly all regions and all target  
 578 months, there is a substantial gap between PM and OP prediction skill, indicating  
 579 a potential for large improvements in regional SIE predictions (see Figs. 9–11). We  
 580 also find that the ACC skill structures are broadly similar between the PM and  
 581 OP predictions. This correspondence indicates that OP prediction skill is partially  
 582 governed by the fundamental predictability limits found in the PM experiments,  
 583 and that common physical mechanisms underlie the prediction skill of both PM  
 584 and OP predictions. Finally, we find that the regional differences in PM prediction  
 585 skill generally mirror the skill differences found in the OP SIE predictions.

586 In both the PM and OP predictions, the highest regional prediction skill is  
 587 found for winter SIE in the North Atlantic sector (see Fig. 9). PM predictions  
 588 in the Barents and GIN Seas are highly skillful (defined here as  $ACC \geq 0.7$ ; a  
 589 prediction capable of capturing more than half the variance) at lead times beyond  
 590 24 months. This lies in contrast to the OP predictions, which have statistically  
 591 significant skill in these regions at lead times of 5–11 months, but are not highly  
 592 skillful. In both PM and OP predictions, regional SIE skill in the North Pacific  
 593 sector is lower than that of the North Atlantic. This suggests that the Bering  
 594 Sea and Sea of Okhotsk are fundamentally less predictable, lacking the potential  
 595 for highly skillful predictions beyond 12-month lead times. Compared with the

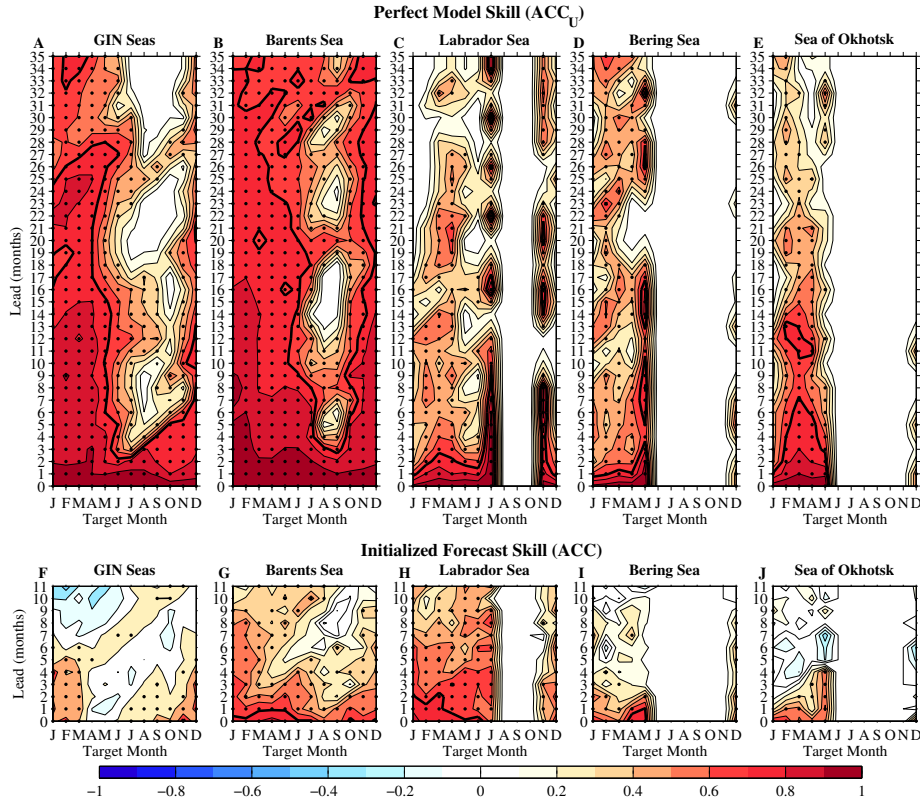


**Fig. 9** Comparison of PM prediction skill ( $ACC_U$ ) and OP prediction skill ( $ACC$ ) for Arctic regional SIE for the GIN, Barents, Labrador, and Bering Seas and the Sea of Okhotsk.  $ACC$  values are plotted as a function of target month and forecast lead time, and are only plotted for target months with SIE standard deviation greater than  $0.03 \times 10^6 \text{ km}^2$ . The thick black lines indicate the  $ACC=0.7$  contours. Dots indicate months in which the  $ACC$  values are statistically significant at the 95% confidence level.

596 large PM/OP skill gap found in other regions, the Labrador Sea is an exception,  
 597 showing similar PM and OP skill. The PM skill of this model may underestimate  
 598 the fundamental limit of Labrador SIE predictability, as this model has too little  
 599 SIC variability in this region (See Fig. S4). This SIC variability bias likely results  
 600 from excessive deep open ocean convection in the Labrador sea, which restricts sea-  
 601 ice variability in this region. Indeed, the study of [21] found that the Labrador Sea  
 602 had the longest duration of predictability in HadGEM1.2, suggesting that model  
 603 formulation and biases may strongly affect Labrador Sea predictability estimates.

604 The study of [12] identified a spring prediction skill barrier in the Laptev, East  
 605 Siberian and Beaufort Seas, in which summer SIE prediction skill dropped off  
 606 sharply for OP forecasts initialized prior to May, May, and June, respectively (see  
 607 Fig. 10g,10h,10j). Interestingly, the PM forecasts show a similar skill barrier in  
 608 these regions, with highly skillful summer SIE predictions for forecasts initialized  
 609 May 1 and later, and a clear drop-off in skill for predictions initialized before this  
 610 (see Fig. 10b,10c,10e). The diagonal ACC contours in these regions indicate that

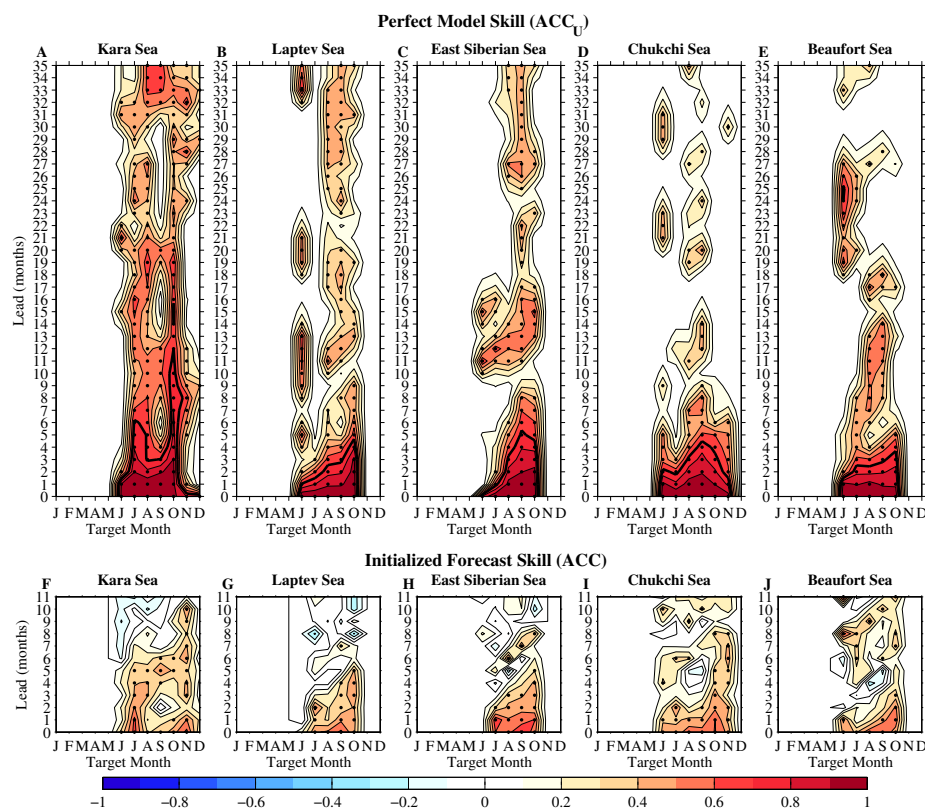


**Fig. 10** Comparison of PM prediction skill ( $ACC_U$ ) and OP prediction skill ( $ACC$ ) for Arctic regional SIE for the Kara, Laptev, East Siberian, Chukchi, and Beaufort Seas.

611 summer SIE skill tends to be roughly constant for a given initialization month.  
 612 The fact that the spring prediction skill barrier is present in both OP and PM  
 613 predictions suggests that it is a fundamental predictability feature of this model,  
 614 rather than resulting from IC errors in the OP predictions. In particular, the  
 615 perfect SIT ICs in the PM experiments are not sufficient to overcome this spring  
 616 barrier. Additional PM experiments using other GCMs are required to determine  
 617 if the spring barrier is truly a feature present in nature. Summer SIE predictions in  
 618 the Chukchi Sea are highly skillful at 2-4 month lead times in the PM experiments.  
 619 While there is some diagonal structure in the Chukchi ACC plots, both the PM  
 620 and OP predictions do not have a clearly defined spring barrier in this region. The  
 621 Kara Sea has highly skillful PM predictions for summer and fall SIE at lead times  
 622 of 2-11 months and also does not show a spring prediction skill barrier.

623 The Central Arctic has relatively low PM and OP prediction skill (see Fig. 11),  
 624 whereas the Canadian Archipelago has slightly higher skill, with highly skillful PM  
 625 forecasts of August and September SIE at 2-3 month lead times. The Canadian  
 626 Archipelago results should be viewed with some caution, given the model's coarse  
 627 resolution of this bathymetrically complex region. The PM forecasts have skill  
 628 in predicting both melt season and growth season SIE anomalies in Hudson and

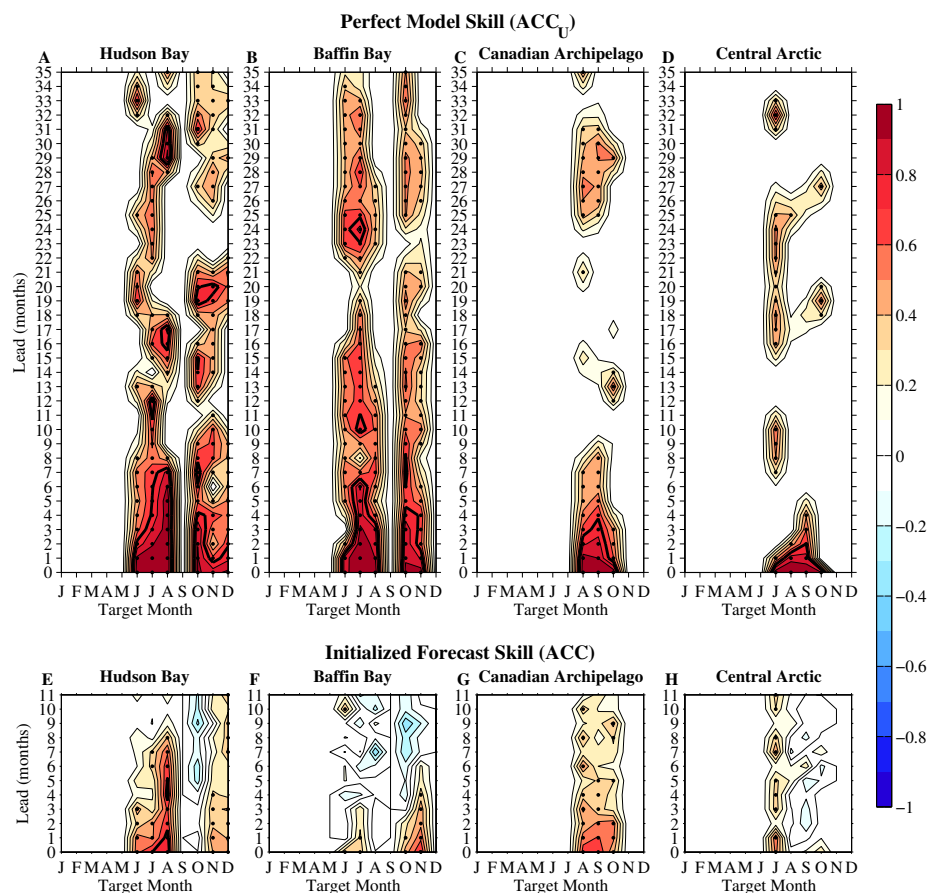


**Fig. 11** Comparison of PM prediction skill ( $ACC_U$ ) and OP prediction skill ( $ACC$ ) for Arctic regional SIE for Hudson Bay, Baffin Bay, the Canadian Arctic Archipelago, and the Central Arctic.

629 Baffin Bay. In each of these regions, the melt season skill is higher than the growth  
 630 season, suggesting that persistence of winter ice thickness anomalies is the greatest  
 631 source of predictability in these regions. The Hudson and Baffin Bay OP skill is  
 632 substantially lower than the PM skill, particularly for the growth season in Hudson  
 633 Bay and the melt season in Baffin Bay. This skill discrepancy could possibly be  
 634 reduced by directly assimilating SIT data in the OP system.

635 We also note that there are a small number of instances in which an isolated  
 636 month shows OP skill but not PM skill (for example, lead-6 September predictions  
 637 in the Barents Sea, lead-8 October/November predictions in the Chukchi Sea, and  
 638 lead-4 November predictions in the Kara Sea). These instances tend to have fairly  
 639 low skill ( $ACC < 0.5$ ), suggesting that sampling errors in the OP predictions could  
 640 be playing a role. Also, in some of these instances the PM skill does not decay  
 641 monotonically with lead time, violating a property that we expect PM predictions  
 642 to satisfy. This suggests that sampling errors in the PM predictions could also  
 643 explain these discrepancies.

## 644 4.3 Interpretation of the PM/OP skill gap

645 The PM/OP skill gap demonstrated in Figs. 9-11 raises a natural question: To  
646 what extent can these PM skill estimates be realized in future OP prediction sys-  
647 tems? In other words, is it valid to interpret the PM/OP skill gap as possible  
648 “room for improvement” in prediction skill? The work of [47] directly addresses  
649 these questions, providing a framework to assess the fidelity of PM skill estimates.  
650 [47] argue that the interpretation of the PM/OP skill gap as “room for improve-  
651 ment” relies on an implicit assumption that the observed and model-predicted  
652 time series’ share the same statistical characteristics. In particular, they show  
653 that differences in PM skill between different models can largely be attributed to  
654 differences in temporal autocorrelation (persistence) and, by extension, argue that  
655 a model’s temporal autocorrelation should be compared to observations before  
656 making inferences based on PM skill.

657 Following this, we compare the temporal autocorrelation of observed detrended  
658 regional SIE to the autocorrelation of the FLOR control run. Computing autocor-  
659 relation values for all target months and lead times of 0-35 months, we find that  
660 the model’s regional SIE persistence characteristics are generally quite consistent  
661 with observed persistence (see Figs. S6-S8). In particular, we find strong agree-  
662 ment in the Laptev, East Siberian, Beaufort, Bering, Canadian Arctic Archipelago,  
663 Hudson Bay, Baffin Bay, and Central Arctic regions. This suggests that in these  
664 regions the PM skill provides a reliable estimate of the true upper limits of skill  
665 achievable in nature. In the Chukchi Sea, Kara Sea, and Sea of Okhotsk, the model  
666 autocorrelation values agree well with observations for lead times less than or equal  
667 to 6 months. For lead times beyond 6 months, the model has higher correlation  
668 values than observed, although the values are quite modest (less than 0.4). Since  
669 the majority of highly skillful PM predictions in these regions occur for lead times  
670 of 6 months or less, we conclude that the PM skill estimates are also quite reliable  
671 in these regions. We find a larger discrepancy in the GIN and Barents Seas, with  
672 the model displaying higher autocorrelation values than the observations, partic-  
673 ularly for winters 1 and 2 years in advance of a given winter target month. This  
674 discrepancy could potentially arise due to the removal of low-frequency (period  
675  $> 20$  years) variability when the observed SIE is linearly detrended. However, we  
676 find that this cannot fully explain the discrepancy, as notable differences in au-  
677 tocorrelation remain present even if the model data is 20-year high-pass filtered.  
678 This suggests that the PM skill may overestimate the true upper limits of pre-  
679 diction skill in the Barents and GIN Seas. Conversely, we find that the model  
680 has lower autocorrelation values than detrended observations in the Labrador Sea,  
681 suggesting that the PM skill underestimates the true skill achievable in this region.  
682 This is consistent with the lack of a PM/OP skill gap in the Labrador Sea, and  
683 likely results from the model biases discussed in subsection 4.2. Finally, we find  
684 that the model’s pan-Arctic SIE is substantially more persistent than detrended  
685 observations, suggesting that the PM skill overestimates the true upper limit of  
686 predictability for the pan-Arctic domain. Overall, these findings provide general  
687 confidence in the interpretation of the PM/OP skill gap as possible “room for im-  
688 provement” in prediction skill, while highlighting some caveats that apply to the  
689 North Atlantic regions and the pan-Arctic domain.

## 690 5 Conclusions and Discussion

691 In this work, we have established the first direct comparison of perfect model  
 692 (PM) and operational (OP) Arctic sea-ice prediction skill within a common pre-  
 693 diction system. Using the GFDL-FLOR coupled GCM, we have performed two  
 694 complementary suites of ensemble prediction experiments. The first is a suite of  
 695 PM experiments, consisting of ensembles initialized in January, March, May, July,  
 696 September, and November, and in high, low, and typical sea-ice volume (SIV)  
 697 regimes. Secondly, we have utilized a suite of retrospective initialized OP predic-  
 698 tions spanning 1981-2016 made with GFDL-FLOR. The skill comparison between  
 699 these OP predictions and the PM experiments forms the basis of this study.

700 In order to make a robust skill comparison, we have introduced a set of PM skill  
 701 metrics, defined in analogy with metrics used in OP prediction applications. These  
 702 metrics were designed to allow for an “apples-to-apples” PM/OP skill comparison,  
 703 and offer conceptual advantages over other commonly used PM skill metrics. We  
 704 have found that PM skill metrics based on ensemble spread (RMSE, NRMSE,  
 705 MSSS) do not have a clear dependence on the SIV state, whereas the  $ACC$  is  
 706 clearly higher in high/low volume states compared with typical volume states.  
 707 This state-dependency can lead to biased  $ACC$  estimates if start dates are not  
 708 sampled from the climatological distribution. We have defined an unbiased  $ACC$ ,  
 709  $ACC_U$ , which does not suffer from this sampling bias. All comparisons with OP  
 710 prediction skill in this study were made using  $ACC_U$ . The unbiased  $ACC$  metric  
 711 may be broadly useful for PM studies, since many of these studies do not sample  
 712 start dates from the climatological distribution of states. Using these PM and OP  
 713 skill metrics, we have investigated the predictability of pan-Arctic SIV, pan-Arctic  
 714 SIE, and regional Arctic SIE.

715 This study has shown that PM predictions of pan-Arctic SIV and SIE have  
 716 statistically significant skill for all target months and lead times up to 35 months  
 717 (the length of our PM simulations). The PM predictions of pan-Arctic SIE are  
 718 highly skillful ( $ACC_U \geq 0.7$ ) at leads of 18–26 months for winter SIE predictions  
 719 and leads of 5–11 months for summer SIE predictions. In contrast, OP predic-  
 720 tions of pan-Arctic SIE have statistically significant skill at lead times of 0–5  
 721 months, and are not highly skillful beyond lead-0. This notable skill gap indicates  
 722 that pan-Arctic SIE predictions could be improved in all months of the year, with  
 723 particularly large opportunities for improvements in winter SIE predictions. Given  
 724 that winter sea ice covaries strongly with the NAO (e.g. [26]) and that SIC anom-  
 725 alies can force an NAO response [25,69], improving winter SIE predictions has the  
 726 potential to improve winter NAO predictions. For example, recent work by [73]  
 727 shows that fall SIC is an important predictor of the winter NAO index, attributing  
 728 their NAO skill to persistence of fall SIC conditions.

729 The uniform seasonal coverage of PM start dates employed by this study has  
 730 allowed us to shed additional light on the spring predictability barrier for pan-  
 731 Arctic SIE proposed by [21]. We have found that PM predictions of pan-Arctic SIV  
 732 display a spring predictability barrier related to rapid error growth during the early  
 733 melt season, in which predictions initialized prior to June lose skill much faster  
 734 than those initialized post June. Unlike SIV, we have found that pan-Arctic SIE  
 735 does not display a clear spring predictability barrier. This finding, which may be  
 736 model-dependent, suggests that there is not an optimal month in which to initialize  
 737 pan-Arctic SIE predictions. While the spring barrier is not present for pan-Arctic

738 SIE, we have found clear evidence of spring predictability barriers in certain Arctic  
739 regions. In particular, the Laptev, East Siberian, and Beaufort Seas each display  
740 spring prediction skill barriers in both the PM and OP predictions, suggesting  
741 that these barriers are a fundamental predictability feature of these regions. These  
742 barriers suggest that summer SIE predictions in these regions should be initialized  
743 May 1 or later, since skill is substantially lower for predictions initialized prior to  
744 May 1.

745 In nearly all Arctic regions, we have identified substantial skill gaps between  
746 PM and OP predictions of Arctic regional SIE. While their absolute skill values are  
747 different, the PM and OP regional predictions generally display similar correlation  
748 skill structures, indicating that similar physical mechanisms are contributing to  
749 both PM and OP skill. We have found that PM predictions in the Barents and GIN  
750 Seas are highly skillful at lead times beyond 24 months, whereas OP predictions  
751 have statistically significant skill at 5-11 months but are not highly skillful beyond  
752 1 month lead times. In both the PM and OP predictions, the North Pacific sector  
753 has lower winter SIE skill than these North Atlantic regions, suggesting that the  
754 North Pacific is fundamentally less predictable. This finding is consistent with the  
755 PM study of [21] and the statistical prediction study of [81], and is relevant for  
756 fisheries industries active in these regions that could benefit from skillful winter  
757 SIE predictions.

758 We have found that regional winter SIE is generally more predictable than  
759 summer SIE. PM predictions of regional summer SIE in the Laptev, East Siberian,  
760 Chukchi, and Beaufort Seas are highly skillful at leads of 1–5 months, displaying  
761 similar correlation structures to their OP counterparts. The PM/OP skill gap  
762 suggests that substantial improvements are possible at these 1–5 month lead times,  
763 but that long-lead skillful predictions are not possible in these regions. This finding  
764 is relevant for the predictability of summer shipping lanes along the Northern Sea  
765 Route, implying that these lanes could be skillfully predicted from May 1, but not  
766 earlier.

767 This study has identified a striking skill gap between OP and PM predictions  
768 made with the GFDL-FLOR model, suggesting that skillful long-lead predictions  
769 of SIE are possible in many regions of the Arctic. The large gap in lead-0 prediction  
770 skill indicates a clear potential for improved predictions via improved initialization.  
771 Additionally, the rapid decay of OP prediction skill relative to the PM experiments  
772 indicates that improved model physics and/or more balanced ICs are required in  
773 future prediction systems. It is important to note that these findings are based  
774 upon a single GCM and similar studies with other seasonal prediction systems  
775 are required to solidify these results. This work has provided a robust comparison  
776 of regional PM and OP prediction skill, but has not investigated the physical  
777 mechanisms underlying this skill. Future work exploring these mechanisms, and  
778 identifying the key modeling and observational deficiencies in current dynamical  
779 prediction systems, is required in order to close the gap between PM and OP skill  
780 identified in this study.

781 **Acknowledgements** This paper is dedicated to Walter Bushuk. We thank two anonymous re-  
782 viewers for constructive comments which improved the manuscript. We also acknowledge Olga  
783 Sergienko and Hiroyuki Murakami for comments on a preliminary version of the manuscript.  
784 We thank Seth Underwood, Bill Hurlin, and Chris Blanton for assistance in setting up the

785 model experiments. M. Bushuk was supported by NOAA's Climate Program Office, Climate  
786 Variability and Predictability Program (Award GC15-504).

## 787 6 Appendix

### 788 6.1 Reliability condition for ensemble forecasts

789 Claim: The PM MSE given by Eqn. 8 satisfies the necessary condition for forecast  
790 reliability:

$$MSE(\tau) = \frac{N}{N-1} \sigma_e^2(\tau). \quad (18)$$

791 Proof: The mean intra-ensemble variance,  $\sigma_e^2$ , is given by

$$\sigma_e^2(\tau) = \frac{1}{M} \sum_{j=1}^M \frac{1}{N-1} \sum_{i=1}^N \left( \langle \mathbf{x}_j(\tau) \rangle - x_{ij}(\tau) \right)^2, \quad (19)$$

792 where  $\langle \mathbf{x}_j(\tau) \rangle$  is the ensemble mean of the  $j$ th ensemble. The MSE is given by

$$MSE(\tau) = \frac{\sum_{j=1}^M \sum_{i=1}^N \left( \langle \mathbf{x}_{i_j}(\tau) \rangle - x_{ij}(\tau) \right)^2}{MN}. \quad (20)$$

793 First, we note a relation between the ensemble mean  $\langle \mathbf{x}_j(\tau) \rangle$  and the ensemble  
794 mean with the  $i$ th member removed  $\langle \mathbf{x}_{i_j}(\tau) \rangle$ . These ensemble means are defined  
795 respectively as

$$\langle \mathbf{x}_j(\tau) \rangle = \frac{1}{N} \sum_{k=1}^N x_{kj}(\tau), \quad (21)$$

796 and

$$\langle \mathbf{x}_{i_j}(\tau) \rangle = \frac{1}{N-1} \sum_{k \neq i}^N x_{kj}(\tau), \quad (22)$$

797 and are related by:

$$\langle \mathbf{x}_j(\tau) \rangle = \frac{1}{N} \sum_{k=1}^N x_{kj}(\tau) = \frac{x_{ij}(\tau)}{N} + \frac{1}{N} \sum_{k \neq i}^N x_{kj}(\tau) = \frac{x_{ij}(\tau)}{N} + \frac{N-1}{N} \langle \mathbf{x}_{i_j}(\tau) \rangle. \quad (23)$$

798 Therefore,

$$\sigma_e^2(\tau) = \frac{\sum_{j=1}^M \sum_{i=1}^N \left( \langle \mathbf{x}_j(\tau) \rangle - x_{ij}(\tau) \right)^2}{M(N-1)} \quad (24)$$

$$= \frac{\sum_{j=1}^M \sum_{i=1}^N \left( \frac{1}{N} x_{ij}(\tau) + \frac{N-1}{N} \langle \mathbf{x}_{i_j}(\tau) \rangle - x_{ij}(\tau) \right)^2}{M(N-1)} \quad (25)$$

$$= \frac{\sum_{j=1}^M \sum_{i=1}^N \left( \frac{N-1}{N} \langle \mathbf{x}_{i_j}(\tau) \rangle - \frac{N-1}{N} x_{ij}(\tau) \right)^2}{M(N-1)} \quad (26)$$

$$= \left( \frac{N-1}{N} \right)^2 \frac{\sum_{j=1}^M \sum_{i=1}^N \left( \langle \mathbf{x}_{i_j}(\tau) \rangle - x_{ij}(\tau) \right)^2}{M(N-1)} \quad (27)$$

$$= \frac{N-1}{N} \frac{\sum_{j=1}^M \sum_{i=1}^N \left( \langle \mathbf{x}_{ij}(\tau) \rangle - x_{ij}(\tau) \right)^2}{MN} \quad (28)$$

$$= \frac{N-1}{N} MSE(\tau). \quad (29)$$

## 799 6.2 Relation of perfect model skill metrics to other metrics

### 800 6.2.1 PPP

801 A commonly used PM skill metric is the potential prognostic predictability (PPP,  
802 [61]), which compares the ensemble variance,  $\sigma_e^2(\tau)$ , to the climatological variance,  
803  $\sigma_c^2$ . The PPP is defined as

$$PPP(\tau) = 1 - \frac{\sigma_e^2(\tau)}{\sigma_c^2}, \quad (30)$$

804 which has a similar form to the MSSS defined in Eqn. 11. Since  $MSE = \frac{N}{N-1} \sigma_e^2$ ,  
805 for any finite  $N$ ,  $MSSS < PPP$  and  $MSSS \rightarrow PPP$  as  $N \rightarrow \infty$ . For most  
806 typical values of  $N$ , the PPP and MSSS will be quite similar and share the same  
807 qualitative interpretations. However, we believe that the  $MSSS$  metric provides  
808 a more natural comparison with the  $MSSS$  metric used in OP predictions. In  
809 the  $PPP$  formulation, the ensemble mean  $\langle x_j \rangle$  is used to predict a given truth  
810 member  $x_{ij}$ . This implies that the prediction has knowledge of the observed value,  
811 since the  $x_{ij}$  truth member is included in the ensemble mean computation. This  
812 is an undesirable property for a skill metric, and will tend to bias skill scores high.  
813 The  $MSSS$  does not suffer from this issue, as only non-truth members are used to  
814 predict a given truth member.

### 815 6.2.2 RMSE

816 In the PM MSE formula given in Eqn. 8, we have used the  $(N - 1)$ -member  
817 ensemble mean to predict a given truth member. In general, we could use an  $E$ -  
818 member ensemble mean to make this prediction, where  $1 \leq E \leq N - 1$ . It can  
819 be shown that an  $MSE$  based on an  $E$ -member ensemble mean satisfies  $MSE =$   
820  $\frac{E+1}{E} \sigma_e^2$ , where the proof uses the Central Limit Theorem and follows the same  
821 approach as that of [41]. The formula in 6.1 is the special case when  $E = N - 1$ .  
822 The PM RMSE definition of [19], uses 1-member ensembles to predict a given truth  
823 member, and therefore satisfies  $MSE = 2\sigma_e^2$ . At long lead times, the PM RMSE  
824 of [19] converges to  $\sqrt{2}\sigma_c$  (note that this is strictly true only if the normalization  
825 of  $MN(N - 1) - 1$  used in [19] is replaced with  $MN(N - 1)$ ).

826 This factor of  $\sqrt{2}$  is a potential source of confusion, since in the PM literature  
827 a “no skill” forecast has  $RMSE = \sqrt{2}\sigma_c$ , whereas in the OP literature a “no skill”  
828 (climatological) forecast has an RMSE of  $\sigma_c$ . This can lead to confusion when  
829 quoting PM RMSE in physical units, or when comparing PM and OP RMSE  
830 values (e.g. as done in [7, 70]). In particular, the RMSE values obtained via the  
831 formula of [19] are too large, since they do not benefit from ensemble averaging. If  
832 ensemble means are used for the PM prediction, this issue is greatly ameliorated,  
833 since the PM RMSE values converge to  $\sqrt{\frac{N}{N-1}}\sigma_c$ , allowing for cleaner comparison  
834 with OP predictions.

## References

- 836 1. Anderson, J.L.: An ensemble adjustment Kalman filter for data assimilation. *Monthly*  
837 *weather review* **129**(12), 2884–2903 (2001)
- 838 2. Bitz, C., Holland, M., Weaver, A., Eby, M.: Simulating the ice-thickness distribution in a  
839 coupled climate model. *J. Geophys. Res.: Oceans* **106**(C2), 2441–2463 (2001)
- 840 3. Bitz, C., Roe, G.: A mechanism for the high rate of sea ice thinning in the Arctic Ocean.  
841 *J. Climate* **17**(18), 3623–3632 (2004)
- 842 4. Blanchard-Wrigglesworth, E., Armour, K.C., Bitz, C.M., DeWeaver, E.: Persistence and  
843 inherent predictability of Arctic sea ice in a GCM ensemble and observations. *J. Climate*  
844 **24**, 231–250 (2011)
- 845 5. Blanchard-Wrigglesworth, E., Barthélemy, A., Chevallier, M., Cullather, R., Fučkar, N.,  
846 Massonnet, F., Posey, P., Wang, W., Zhang, J., Ardilouze, C., et al.: Multi-model seasonal  
847 forecast of Arctic sea-ice: forecast uncertainty at pan-Arctic and regional scales. *Climate*  
848 *Dynamics* **49**(4), 1399–1410 (2017)
- 849 6. Blanchard-Wrigglesworth, E., Bitz, C., Holland, M.: Influence of initial conditions and  
850 climate forcing on predicting Arctic sea ice. *Geophys. Res. Lett.* **38**(18) (2011)
- 851 7. Blanchard-Wrigglesworth, E., Cullather, R., Wang, W., Zhang, J., Bitz, C.: Model forecast  
852 skill and sensitivity to initial conditions in the seasonal Sea Ice Outlook. *Geophys. Res.*  
853 *Lett* **42**(19), 8042–8048 (2015)
- 854 8. Bretherton, C.S., Widmann, M., Dymnikov, V.P., Wallace, J.M., Bladé, I.: The effective  
855 number of spatial degrees of freedom of a time-varying field. *J. Climate* **12**(7), 1990–2009  
856 (1999)
- 857 9. Bushuk, M., Giannakis, D.: Sea-ice reemergence in a model hierarchy. *Geophys. Res. Lett.*  
858 **42**, 5337–5345 (2015)
- 859 10. Bushuk, M., Giannakis, D.: The seasonality and interannual variability of Arctic sea-ice  
860 reemergence. *J. Climate* **30**, 4657–4676 (2017)
- 861 11. Bushuk, M., Giannakis, D., Majda, A.J.: Arctic sea-ice reemergence: The role of large-scale  
862 oceanic and atmospheric variability. *J. Climate* **28**, 5477–5509 (2015)
- 863 12. Bushuk, M., Msadek, R., Winton, M., Vecchi, G., Gudgel, R., Rosati, A., Yang, X.: Skillful  
864 regional prediction of Arctic sea ice on seasonal timescales. *Geophys. Res. Lett.* **44** (2017)
- 865 13. Bushuk, M., Msadek, R., Winton, M., Vecchi, G., Gudgel, R., Rosati, A., Yang, X.: Summer  
866 enhancement of Arctic sea-ice volume anomalies in the September-ice zone. *J. Climate*  
867 **30**, 2341–2362 (2017)
- 868 14. Cavalieri, D.J., Parkinson, C.L., Gloersen, P., Zwally, H.J.: Sea ice concentrations from  
869 Nimbus-7 SMMR and DMSP SSM/I-SSMIS Passive Microwave Data, Version 1. NASA  
870 DAAC at the Natl. Snow and Ice Data Cent. (1996). DOI 10.5067/8GQ8LZQVL0VL
- 871 15. Chen, Z., Liu, J., Song, M., Yang, Q., Xu, S.: Impacts of assimilating satellite sea ice  
872 concentration and thickness on Arctic sea ice prediction in the NCEP Climate Forecast  
873 System. *Journal of Climate* **30**(21), 8429–8446 (2017)
- 874 16. Cheng, W., Blanchard-Wrigglesworth, E., Bitz, C.M., Ladd, C., Stabenro, P.J.: Diagnostic  
875 sea ice predictability in the pan-Arctic and US Arctic regional seas. *Geophys. Res. Lett.*  
876 **43**(22) (2016)
- 877 17. Chevallier, M., Salas y Mélia, D.: The role of sea ice thickness distribution in the Arctic  
878 sea ice potential predictability: A diagnostic approach with a coupled GCM. *J. Climate*  
879 **25**(8), 3025–3038 (2012)
- 880 18. Chevallier, M., Salas y Mélia, D., Voldoire, A., Déqué, M., Garric, G.: Seasonal forecasts of  
881 the pan-Arctic sea ice extent using a GCM-based seasonal prediction system. *J. Climate*  
882 **26**(16), 6092–6104 (2013)
- 883 19. Collins, M.: Climate predictability on interannual to decadal time scales: The initial value  
884 problem. *Climate Dyn.* **19**, 671–692 (2002)
- 885 20. Collow, T.W., Wang, W., Kumar, A., Zhang, J.: Improving Arctic sea ice prediction using  
886 PIOMAS initial sea ice thickness in a coupled ocean–atmosphere model. *Mon. Wea. Rev.*  
887 **143**(11), 4618–4630 (2015)
- 888 21. Day, J., Tietsche, S., Hawkins, E.: Pan-Arctic and regional sea ice predictability: Initial-  
889 ization month dependence. *J. Climate* **27**(12), 4371–4390 (2014)
- 890 22. Day, J.J., Goessling, H.F., Hurlin, W.J., Keeley, S.P.: The Arctic predictability and predic-  
891 tion on seasonal-to-interannual timescales (APPOSITE) data set version 1. *Geoscientific*  
892 *Model Development* **9**(6), 2255 (2016)

- 893 23. Delworth, T.L., Broccoli, A.J., Rosati, A., Stouffer, R.J., Balaji, V., Beesley, J.A., Cooke,  
894 W.F., Dixon, K.W., Dunne, J., Dunne, K., et al.: GFDL's CM2 global coupled climate  
895 models. Part I: Formulation and simulation characteristics. *J. Climate* **19**(5), 643–674  
896 (2006)
- 897 24. Delworth, T.L., Rosati, A., Anderson, W., Adcroft, A.J., Balaji, V., Benson, R., Dixon, K.,  
898 Griffies, S.M., Lee, H.C., Pacanowski, R.C., et al.: Simulated climate and climate change  
899 in the GFDL CM2.5 high-resolution coupled climate model. *J. Climate* **25**(8), 2755–2781  
900 (2012)
- 901 25. Deser, C., Magnusdottir, G., Saravanan, R., Phillips, A.: The effects of North Atlantic  
902 SST and sea ice anomalies on the winter circulation in CCM3. Part II: Direct and indirect  
903 components of the response. *Journal of Climate* **17**(5), 877–889 (2004)
- 904 26. Deser, C., Walsh, J.E., Timlin, M.S.: Arctic sea ice variability in the context of recent  
905 atmospheric circulation trends. *J. Climate* **13**, 617–633 (2000)
- 906 27. Dirkson, A., Merryfield, W.J., Monahan, A.: Impacts of sea ice thickness initialization on  
907 seasonal Arctic sea ice predictions. *Journal of Climate* **30**(3), 1001–1017 (2017)
- 908 28. Drobot, S.D.: Using remote sensing data to develop seasonal outlooks for Arctic regional  
909 sea-ice minimum extent. *Remote Sensing of Environment* **111**(2-3), 136–147 (2007)
- 910 29. Drobot, S.D., Maslanik, J.A., Fowler, C.: A long-range forecast of Arctic summer sea-ice  
911 minimum extent. *Geophysical Research Letters* **33**(10) (2006)
- 912 30. Germe, A., Chevallier, M., y Méliá, D.S., Sanchez-Gomez, E., Cassou, C.: Interannual  
913 predictability of Arctic sea ice in a global climate model: Regional contrasts and temporal  
914 evolution. *Climate Dynamics* **43**(9-10), 2519–2538 (2014)
- 915 31. Griffies, S.: Elements of the Modular Ocean Model (MOM), GFDL Ocean Group Technical  
916 Report. Tech. Rep. No. 7, NOAA/Geophysical Fluid Dynamics Laboratory (2012)
- 917 32. Griffies, S.M., Winton, M., Donner, L.J., Horowitz, L.W., Downes, S.M., Farneti, R.,  
918 Gnanadesikan, A., Hurlin, W.J., Lee, H.C., Liang, Z., et al.: The GFDL CM3 coupled  
919 climate model: characteristics of the ocean and sea ice simulations. *Journal of Climate*  
920 **24**(13), 3520–3544 (2011)
- 921 33. Guemas, V., Chevallier, M., Dqu, M., Bellprat, O., Doblas-Reyes, F.: Impact of sea ice  
922 initialisation on sea ice and atmosphere prediction skill on seasonal timescales. *Geophys.*  
923 *Res. Lett* **43**(8), 3889–3896 (2016)
- 924 34. Hawkins, E., Tietsche, S., Day, J.J., Melia, N., Haines, K., Keeley, S.: Aspects of design-  
925 ing and evaluating seasonal-to-interannual Arctic sea-ice prediction systems. *Quarterly*  
926 *Journal of the Royal Meteorological Society* **142**(695), 672–683 (2016)
- 927 35. Holland, M.M., Bailey, D.A., Vavrus, S.: Inherent sea ice predictability in the rapidly  
928 changing Arctic environment of the Community Climate System Model, version 3. *Climate*  
929 *Dynamics* **36**(7-8), 1239–1253 (2011)
- 930 36. Holland, M.M., Stroeve, J.: Changing seasonal sea ice predictor relationships in a changing  
931 arctic climate. *Geophys. Res. Lett* **38**(18) (2011)
- 932 37. Hunke, E., Dukowicz, J.: An elastic-viscous-plastic model for sea ice dynamics. *J. Phys.*  
933 *Oceanogr.* **27**(9), 1849–1867 (1997)
- 934 38. Jia, L., Yang, X., Vecchi, G., Gudgel, R., Delworth, T., Fueglistaler, S., Lin, P., Scaife,  
935 A.A., Underwood, S., Lin, S.J.: Seasonal prediction skill of northern extratropical surface  
936 temperature driven by the stratosphere. *Journal of Climate* **30**(1), 4463–4475 (2017)
- 937 39. Jia, L., Yang, X., Vecchi, G.A., Gudgel, R.G., Delworth, T.L., Rosati, A., Stern, W.F.,  
938 Wittenberg, A.T., Krishnamurthy, L., Zhang, S., et al.: Improved seasonal prediction of  
939 temperature and precipitation over land in a high-resolution GFDL climate model. *J.*  
940 *Climate* **28**(5), 2044–2062 (2015)
- 941 40. Johnson, C., Bowler, N.: On the reliability and calibration of ensemble forecasts. *Monthly*  
942 *Weather Review* **137**(5), 1717–1720 (2009)
- 943 41. Jolliffe, I.T., Stephenson, D.B.: Forecast verification: a practitioner's guide in atmospheric  
944 science—2nd Ed. John Wiley & Sons (2012)
- 945 42. Jung, T., Gordon, N.D., Bauer, P., Bromwich, D.H., Chevallier, M., Day, J.J., Dawson, J.,  
946 Doblas-Reyes, F., Fairall, C., Goessling, H.F., et al.: Advancing polar prediction capabili-  
947 ties on daily to seasonal time scales. *Bull. Amer. Meteor. Soc.* (2016). DOI 10.1175/BAMS-  
948 D-14-00246.1
- 949 43. Kapsch, M.L., Graverson, R.G., Economou, T., Tjernström, M.: The importance of spring  
950 atmospheric conditions for predictions of the Arctic summer sea ice extent. *Geophysical*  
951 *Research Letters* **41**(14), 5288–5296 (2014)
- 952 44. Kauker, F., Kaminski, T., Karcher, M., Giering, R., Gerdes, R., Voßbeck, M.: Adjoint  
953 analysis of the 2007 all time Arctic sea-ice minimum. *Geophysical Research Letters* **36**(3)  
954 (2009)

- 955 45. Koenigk, T., Mikolajewicz, U.: Seasonal to interannual climate predictability in mid and  
956 high northern latitudes in a global coupled model. *Climate dynamics* **32**(6), 783–798  
957 (2009)
- 958 46. Krikken, F., Schmeits, M., Vlot, W., Guemas, V., Hazeleger, W.: Skill improvement of  
959 dynamical seasonal Arctic sea ice forecasts. *Geophys. Res. Lett.* (2016)
- 960 47. Kumar, A., Peng, P., Chen, M.: Is there a relationship between potential and actual skill?  
961 *Monthly Weather Review* **142**(6), 2220–2227 (2014)
- 962 48. Leutbecher, M., Palmer, T.N.: Ensemble forecasting. *Journal of Computational Physics*  
963 **227**(7), 3515–3539 (2008)
- 964 49. Lin, S.J.: A vertically Lagrangian finite-volume dynamical core for global models. *Monthly*  
965 *Weather Review* **132**(10), 2293–2307 (2004)
- 966 50. Lindsay, R., Zhang, J., Schweiger, A., Steele, M.: Seasonal predictions of ice extent in the  
967 Arctic Ocean. *Journal of Geophysical Research: Oceans* **113**(C2) (2008)
- 968 51. Martinson, D.G.: Evolution of the Southern Ocean winter mixed layer and sea ice: Open  
969 ocean deepwater formation and ventilation. *Journal of Geophysical Research: Oceans*  
970 **95**(C7), 11,641–11,654 (1990)
- 971 52. Merryfield, W., Lee, W.S., Wang, W., Chen, M., Kumar, A.: Multi-system seasonal pre-  
972 dictions of Arctic sea ice. *Geophys. Res. Lett.* **40**(8), 1551–1556 (2013)
- 973 53. Milly, P.C., Malyshev, S.L., Shevliakova, E., Dunne, K.A., Findell, K.L., Gleeson, T.,  
974 Liang, Z., Philipps, P., Stouffer, R.J., Swenson, S.: An enhanced model of land water  
975 and energy for global hydrologic and earth-system studies. *Journal of Hydrometeorology*  
976 **15**(5), 1739–1761 (2014)
- 977 54. Msadek, R., Vecchi, G., Winton, M., Gudgel, R.: Importance of initial conditions in sea-  
978 sonal predictions of Arctic sea ice extent. *Geophys. Res. Lett.* **41**(14), 5208–5215 (2014)
- 979 55. Murakami, H., Vecchi, G.A., Delworth, T.L., Wittenberg, A.T., Underwood, S., Gudgel,  
980 R., Yang, X., Jia, L., Zeng, F., Paffendorf, K., et al.: Dominant role of subtropical Pacific  
981 warming in extreme Eastern Pacific hurricane seasons: 2015 and the future. *Journal of*  
982 *Climate* **30**(1), 243–264 (2017)
- 983 56. Murphy, A.H.: Skill scores based on the mean square error and their relationships to the  
984 correlation coefficient. *Monthly weather review* **116**(12), 2417–2424 (1988)
- 985 57. Owens, W.B., Lemke, P.: Sensitivity studies with a sea ice-mixed layer-pycnocline model  
986 in the Weddell sea. *J. Geophys. Res: Oceans* (1978–2012) **95**(C6), 9527–9538 (1990)
- 987 58. Palmer, T., Buizza, R., Hagedorn, R., Lawrence, A., Leutbecher, M., Smith, L.: Ensemble  
988 prediction: a pedagogical perspective. *ECMWF newsletter* **106**, 10–17 (2006)
- 989 59. Peterson, K.A., Arribas, A., Hewitt, H., Keen, A., Lea, D., McLaren, A.: Assessing the  
990 forecast skill of Arctic sea ice extent in the GloSea4 seasonal prediction system. *Climate*  
991 *Dynamics* **44**(1-2), 147–162 (2015)
- 992 60. Petty, A.A., Schröder, D., Stroeve, J., Markus, T., Miller, J., Kurtz, N., Feltham, D.,  
993 Flocco, D.: Skillful spring forecasts of September Arctic sea ice extent using passive mi-  
994 crowave sea ice observations. *Earth's Future* **5**(2), 254–263 (2017)
- 995 61. Pohlmann, H., Botzet, M., Latif, M., Roesch, A., Wild, M., Tschuck, P.: Estimating the  
996 decadal predictability of a coupled AOGCM. *Journal of Climate* **17**(22), 4463–4472 (2004)
- 997 62. Putman, W.M., Lin, S.J.: Finite-volume transport on various cubed-sphere grids. *Journal*  
998 *of Computational Physics* **227**(1), 55–78 (2007)
- 999 63. Schröder, D., Feltham, D.L., Flocco, D., Tsamados, M.: September Arctic sea-ice minimum  
1000 predicted by spring melt-pond fraction. *Nature Climate Change* (2014)
- 1001 64. Schweiger, A., Lindsay, R., Zhang, J., Steele, M., Stern, H., Kwok, R.: Uncertainty in  
1002 modeled Arctic sea ice volume. *J. Geophys. Res.: Oceans* **116**(C8) (2011)
- 1003 65. Sigmond, M., Fyfe, J., Flato, G., Kharin, V., Merryfield, W.: Seasonal forecast skill of  
1004 Arctic sea ice area in a dynamical forecast system. *Geophys. Res. Lett.* **40**(3), 529–534  
1005 (2013)
- 1006 66. Sigmond, M., Reader, M., Flato, G., Merryfield, W., Tivy, A.: Skillful seasonal forecasts  
1007 of Arctic sea ice retreat and advance dates in a dynamical forecast system. *Geophys. Res.*  
1008 *Lett.* **43** (2016)
- 1009 67. Stock, C.A., Pegion, K., Vecchi, G.A., Alexander, M.A., Tommasi, D., Bond, N.A., Fratantoni,  
1010 P.S., Gudgel, R.G., Kristiansen, T., O'Brien, T.D., et al.: Seasonal sea surface temper-  
1011 ature anomaly prediction for coastal ecosystems. *Progress in Oceanography* **137**, 219–236  
1012 (2015)
- 1013 68. Stroeve, J., Hamilton, L.C., Bitz, C.M., Blanchard-Wrigglesworth, E.: Predicting Septem-  
1014 ber sea ice: Ensemble skill of the SEARCH sea ice outlook 2008–2013. *Geophys. Res. Lett.*  
1015 **41**(7), 2411–2418 (2014)

- 1016 69. Sun, L., Deser, C., Tomas, R.A.: Mechanisms of stratospheric and tropospheric circulation  
1017 response to projected Arctic sea ice loss. *Journal of Climate* **28**(19), 7824–7845 (2015)
- 1018 70. Tietsche, S., Day, J., Guemas, V., Hurlin, W., Keeley, S., Matei, D., Msadek, R., Collins,  
1019 M., Hawkins, E.: Seasonal to interannual Arctic sea ice predictability in current global  
1020 climate models. *Geophys. Res. Lett.* **41**(3), 1035–1043 (2014)
- 1021 71. Tivy, A., Howell, S.E., Alt, B., Yackel, J.J., Carrieres, T.: Origins and levels of seasonal  
1022 forecast skill for sea ice in Hudson Bay using Canonical Correlation Analysis. *Journal of*  
1023 *Climate* **24**(5), 1378–1395 (2011)
- 1024 72. Vecchi, G.A., Delworth, T., Gudgel, R., Kapnick, S., Rosati, A., Wittenberg, A.T., Zeng,  
1025 F., Anderson, W., Balaji, V., Dixon, K., et al.: On the seasonal forecasting of regional  
1026 tropical cyclone activity. *J. Climate* **27**(21), 7994–8016 (2014)
- 1027 73. Wang, L., Ting, M., Kushner, P.: A robust empirical seasonal prediction of winter NAO  
1028 and surface climate. *Scientific Reports* **7**(1), 279 (2017)
- 1029 74. Wang, L., Yuan, X., Ting, M., Li, C.: Predicting summer Arctic sea ice concentration  
1030 intraseasonal variability using a vector autoregressive model\*. *J. Climate* **29**(4), 1529–  
1031 1543 (2016)
- 1032 75. Wang, W., Chen, M., Kumar, A.: Seasonal prediction of Arctic sea ice extent from a  
1033 coupled dynamical forecast system. *Mon. Wea. Rev.* **141**(4), 1375–1394 (2013)
- 1034 76. Weigel, A.P., Liniger, M.A., Appenzeller, C.: Seasonal ensemble forecasts: Are recalibrated  
1035 single models better than multimodels? *Monthly Weather Review* **137**(4), 1460–1479  
1036 (2009)
- 1037 77. Williams, J., Tremblay, B., Newton, R., Allard, R.: Dynamic preconditioning of the mini-  
1038 mum September sea-ice extent. *J. Climate* **29**(16), 5879–5891 (2016)
- 1039 78. Winton, M.: A reformulated three-layer sea ice model. *J. Atmos. Oceanic Technol.* **17**(4),  
1040 525–531 (2000)
- 1041 79. Yang, X., Vecchi, G.A., Gudgel, R.G., Delworth, T.L., Zhang, S., Rosati, A., Jia, L., Stern,  
1042 W.F., Wittenberg, A.T., Kapnick, S., et al.: Seasonal predictability of extratropical storm  
1043 tracks in GFDLs high-resolution climate prediction model. *Journal of Climate* **28**(9),  
1044 3592–3611 (2015)
- 1045 80. Yeager, S.G., Karspeck, A.R., Danabasoglu, G.: Predicted slowdown in the rate of Atlantic  
1046 sea ice loss. *Geophysical Research Letters* **42**(24) (2015)
- 1047 81. Yuan, X., Chen, D., Li, C., Wang, L., Wang, W.: Arctic sea ice seasonal prediction by a  
1048 linear markov model. *J. Climate* **29**(22), 8151–8173 (2016)
- 1049 82. Zhang, J., Rothrock, D.: Modeling global sea ice with a thickness and enthalpy distribution  
1050 model in generalized curvilinear coordinates. *Mon. Wea. Rev.* **131**(5), 845–861 (2003)
- 1051 83. Zhang, S., Harrison, M., Rosati, A., Wittenberg, A.: System design and evaluation of  
1052 coupled ensemble data assimilation for global oceanic climate studies. *Mon. Wea. Rev.*  
1053 **135**(10), 3541–3564 (2007)
- 1054 84. Zhang, S., Rosati, A.: An inflated ensemble filter for ocean data assimilation with a biased  
1055 coupled GCM. *Mon. Wea. Rev.* **138**(10), 3905–3931 (2010)